1 **Influence of Seed Aerosol Surface Area and Oxidation Rate on Vapor-Wall**
2 **Deposition and SOA Mass Yields: A case study with α-pinene Ozonolysis**

4 T. Nah,[1] R. C. McVay,[2] X. Zhang,[3,#] C. M. Boyd,[1] J. H. Seinfeld[2,3] and N. L. Ng[1,4*]
5
6 [1]*School of Chemical and Biomolecular Engineering, Georgia Institute of Technology, Atlanta, GA, USA*
7 [2]*Division of Chemistry and Chemical Engineering, California Institute of Technology, Pasadena, CA, USA*
8 [3]*Division of Engineering and Applied Science, California Institute of Technology, Pasadena, CA, USA*
9 [4]*School of Earth and Atmospheric Sciences, Georgia Institute of Technology, Atlanta, GA, USA*
10 [#]*Now at: Center for Aerosol and Cloud Chemistry, Aerodyne Research, Billerica, MA, USA*
11
12 ** To whom correspondence should be addressed: ng@chbe.gatech.edu*

14 **Abstract**

15 Laboratory chambers, invaluable in atmospheric chemistry and aerosol formation studies,

16 are subject to particle and vapor wall deposition, processes that need to be accounted for

17 in order to accurately determine secondary organic aerosol (SOA) mass yields. Although

18 particle wall deposition is reasonably well understood and usually accounted for, vapor

19 wall deposition is less so. The effects of vapor wall deposition on SOA mass yields in

20 chamber experiments can be constrained experimentally by increasing the seed aerosol

21 surface area to promote the preferential condensation of SOA-forming vapors onto seed

22 aerosol. Here, we study the influence of seed aerosol surface area and oxidation rate on

23 SOA formation in α-pinene ozonolysis. The observations are analyzed using a coupled

24 vapor-particle dynamics model to interpret the roles of gas-particle partitioning (quasi-

25 equilibrium vs. kinetically-limited SOA growth) and α-pinene oxidation rate in

26 influencing vapor wall deposition. We find that the SOA growth rate and mass yields are

27 independent of seed surface area within the range of seed surface area concentrations

28 used in this study. This behavior arises when the condensation of SOA-forming vapors is

29 dominated by quasi-equilibrium growth. Faster α-pinene oxidation rates and higher SOA

30 mass yields are observed at increasing O_3 concentrations for the same initial α-pinene

31 concentration. When the α-pinene oxidation rate increases relative to vapor wall

32 deposition, rapidly produced SOA-forming oxidation products condense more readily

33 onto seed aerosol particles, resulting in higher SOA mass yields. Our results indicate that

34 the extent to which vapor wall deposition affects SOA mass yields depends on the

35   particular VOC system, and can be mitigated through the use of excess oxidant
36   concentrations.

37   **1. Introduction**

38   Secondary organic aerosol (SOA), formed from the oxidation of volatile and
39   intermediate volatility organic compounds (VOCs and IVOCs), contributes a significant
40   fraction of the global organic aerosol burden (Kanakidou et al., 2005; Hallquist et al.,
41   2009; Tsigaridis et al., 2014). SOA formation studies, which are typically conducted in
42   laboratory chambers in the presence of seed aerosol particles, provide fundamental data
43   that can be used to predict the rate of atmospheric SOA formation. An essential
44   parameter of interest in laboratory chamber studies is the SOA mass yield (Y), which is
45   defined as the ratio of mass concentration of SOA formed to mass concentration of parent
46   hydrocarbon reacted ((ΔHC), $Y = \Delta M_o/\Delta HC$ (Odum et al., 1996; Odum et al., 1997a;
47   Odum et al., 1997b)). The measured SOA mass yields can subsequently be applied in
48   atmospheric models to predict regional and global organic aerosol burdens. In order to
49   obtain accurate SOA mass yields from the evolving aerosol size distribution in chamber
50   experiments, the loss of both particles and vapors to the chamber walls needs to be
51   accurately accounted for (Crump and Seinfeld, 1981; McMurry and Grosjean, 1985;
52   McMurry and Rader, 1985; Cocker et al., 2001a; Weitkamp et al., 2007; Pierce et al.,
53   2008; Hildebrandt et al., 2009; Loza et al., 2010; Matsunaga and Ziemann, 2010; Loza et
54   al., 2012; Kokkola et al., 2014; McVay et al., 2014; Yeh and Ziemann, 2014; Zhang et
55   al., 2014; Yeh and Ziemann, 2015; Zhang et al., 2015a; La et al., 2016).

56   The mechanisms by which particles in chambers deposit on chamber walls are
57   reasonably well understood. Particles are transported to the boundary layer on the
58   chamber walls via diffusion, gravitational settling, and electrostatic forces (Crump and
59   Seinfeld, 1981; McMurry and Grosjean, 1985; McMurry and Rader, 1985; Pierce et al.,
60   2008). The rate at which particles are transported to the edge of the boundary layer is
61   dictated primarily by mixing conditions in the chamber. An effective approach for
62   characterizing particle wall loss involves measuring the size-dependent wall loss rates of
63   polydisperse inert seed aerosol (e.g. ammonium sulfate particles) injected into the
64   chamber during seed-only experiments (Keywood et al., 2004; Pierce et al., 2008). The

65   observed particle number concentration decay in each size bin is then fitted to a first-

66   order exponential decay from which the first-order wall loss coefficients are determined

67   as a function of particle size. These wall loss coefficients are subsequently used to correct

68   for size-dependent particle wall loss in actual SOA formation experiments.

69   Vapor-wall deposition mechanisms in chambers are not as well understood or

70   accounted for as those for particles. The degree to which SOA-forming vapors deposit

71   onto chamber walls is governed by the rate at which these gas-phase organic molecules

72   are transported to the walls, the strength of adherence of the organic molecule to the wall,

73   and the extent of reversible vapor-wall partitioning (Loza et al., 2010; Matsunaga and

74   Ziemann, 2010; Zhang et al., 2015a). For example, Loza et al. (2010) showed that the

75   loss of 2,3-epoxy-1,4-butanediol, an isoprene oxidation product analogue, to walls in the

76   Caltech chamber was essentially irreversible on short time scales but became reversible

77   on longer time scales. In contrast, glyoxal, a common isoprene oxidation product,

78   exhibited reversible vapor-wall partitioning over all time scales. Recent studies show that

79   SOA mass yields measured in chamber experiments can be significantly underestimated

80   due to wall deposition of SOA-forming vapors that would otherwise contribute to SOA

81   growth (McVay et al., 2014; Zhang et al., 2014; La et al., 2016). Zhang et al. (2014)

82   found that chamber-derived SOA mass yields from toluene photooxidation may be

83   underestimated by as much as a factor of four as a result of vapor wall loss.

84   Consequently, the use of underestimated chamber-derived SOA mass yields in

85   atmospheric models will lead to the underprediction of ambient SOA mass concentrations

86   (Cappa et al., 2016).

87   For the toluene photooxidation system, Zhang et al. (2014) showed that the

88   measured SOA mass yields increased with increasing seed aerosol surface area,

89   demonstrating that increasing the seed-to-chamber surface area ratio promoted the

90   condensation of SOA-forming vapors onto seed aerosol particles. However, increasing

91   the seed aerosol surface area to promote condensation of SOA-forming vapors onto seed

92   aerosol particles may not be effective in all VOC oxidation systems. A modeling study by

93   McVay et al. (2014) showed that the SOA mass yield depends on seed aerosol surface

94   area only in cases where the condensation of SOA-forming vapors onto seed aerosol

95   particles is kinetically limited (i.e., the timescale for gas-particle equilibrium is

96   competitive with or greater than the timescale for reaction and vapor-wall deposition). In

97   addition to the seed aerosol surface area, VOC oxidation rate may also play an important

98   role in the effect of vapor wall loss on SOA formation. Ng et al. (2007) showed that the

99   SOA mass yields from *m*-xylene photooxidation are dependent on the oxidation rate, with

100   higher OH concentrations (hence faster oxidation rates) resulting in higher SOA mass

101   yields. It was suggested that the "oxidation rate effect" could arise as a result of

102   competition between growing particles and chamber walls for condensable VOC

103   oxidation products (Ng et al., 2007). However, McVay et al. (2016) reported similar SOA

104   growth at low and high OH concentrations in α-pinene photooxidation. Taken together,

105   these studies show the importance of understanding how gas-particle partitioning and

106   VOC oxidation rate impact vapor-wall deposition and SOA mass yields in laboratory

107   chamber experiments.

108   In this study, we examine the influence of seed aerosol surface area and oxidation

109   rate on SOA formation in α-pinene ozonolysis chamber experiments. α-pinene is the most

110   abundant monoterpene, with global emissions estimated to be ~66 Tg yr^{-1} (Guenther et

111   al., 2012). Ozonolysis is the major atmospheric oxidation pathway of α-pinene, and is

112   estimated to account for reaction of ~46 % of emitted α-pinene (Griffin et al., 1999;

113   Capouet et al., 2008). α-pinene ozonolysis, a major source of atmospheric SOA on both

114   regional and global scales (Kanakidou et al., 2005; Hallquist et al., 2009; Carlton et al.,

115   2010; Pye et al., 2010), has been the subject of numerous studies (Hoffmann et al., 1997;

116   Griffin et al., 1999; Cocker et al., 2001b; Gao et al., 2004; Presto et al., 2005; Presto and

117   Donahue, 2006; Pathak et al., 2007a; Pathak et al., 2007b; Song et al., 2007; Shilling et

118   al., 2008; Henry et al., 2012; Ehn et al., 2014; Kristensen et al., 2014; Zhang et al.,

119   2015b). Here, we measure the α-pinene SOA mass yield as a function of seed aerosol

120   surface area concentration (0 to 3000 μm^2 cm^{-3}) and O$_3$ mixing ratio (100 vs. 500 ppb).

121   These results are analyzed using a coupled vapor-particle dynamics model to evaluate the

122   roles of gas-particle partitioning and VOC oxidation rate in influencing vapor-wall

123   deposition effects on the measured SOA mass yields.

124   **2. Experimental**

2.1. Dark α-pinene ozonolysis experiments

Experiments were conducted in the Georgia Tech Environmental Chamber (GTEC) facility. Details of the dual chamber facility are provided elsewhere (Boyd et al., 2015). Only one FEP Teflon chamber (volume 13 m^3) was used for the entirety of this study. Before each experiment, the chamber is flushed with dried, purified air for at least 36 h until the aerosol number concentration is < 30 cm^{-3}. All experiments were conducted under dry conditions (< 5 % RH) at room temperature (25 °C). NO$_x$ mixing ratios in these experiments are < 1 ppb. Experimental conditions are summarized in Table 1.

22 ppm of cyclohexane (Sigma Aldrich, ≥ 99.9 %) was first injected into the chamber to act as an OH scavenger (~440 times the initial α-pinene concentration). After the cyclohexane concentration had stabilized in the chamber for 30 min, a known concentration (~50 ppb in all experiments) of α-pinene (Sigma Aldrich, > 99 %) was injected into the chamber, followed by inorganic seed aerosol via atomization of an aqueous ammonium sulfate (AS) solution (in seeded experiments). To vary the seed aerosol surface area, different concentrations of AS solutions were used to generate seed aerosol particles in the seeded experiments. In the "low AS" experiments, a 0.015 M AS solution was used to generate seed particles, and the resulting initial total AS seed surface area concentration was ~1000 μm^2 cm^{-3}. In the "high AS" experiments, a 0.05 M AS solution was used to generate seed aerosol particles, and the resulting initial total AS seed surface area concentration was ~3000 μm^2 cm^{-3}. In selected experiments, no seed aerosol particles were introduced into the chamber and SOA was formed via nucleation. After the seed aerosol concentration in the chamber stabilized, O$_3$ (100 or 500 ppb), which was generated by passing purified air into a photochemical cell (Jelight 610), was introduced into the chamber. The start of O$_3$ injection into the chamber marked the beginning of the reaction (i.e., reaction time = 0 min). The initial α-pinene:O$_3$ molar ratio was fixed at approximately 1:2 and 1:10 in the 100 and 500 ppb O$_3$ experiments, respectively. O$_3$ was injected into the chamber for 13.5 and 54.25 min in the 100 and 500 ppb O$_3$ experiments, respectively, to achieve the desired O$_3$ concentrations. The O$_3$ injection times were established in separate experiments in which only O$_3$ was injected into the chamber.

154   The α-pinene and O₃ concentrations were measured by a Gas Chromatograph-

155   Flame Ionization Detector (GC-FID, Agilent 7890A) and O₃ monitor (Teledyne T400),

156   respectively. GC-FID measurements were taken 12 min apart. A High Resolution Time-

157   of-Flight Aerosol Mass Spectrometer (HR-ToF-AMS, Aerodyne Research Inc.) was used

158   to measure the aerosol elemental composition (DeCarlo et al., 2006; Canagaratna et al.,

159   2015). Details on the operation of the HR-ToF-AMS and its data analysis are described

160   elsewhere (Canagaratna et al., 2015). Aerosol size distributions, number and volume

161   concentrations were measured by a Scanning Mobility Particle Sizer (SMPS, TSI), which

162   consists of a Differential Mobility Analyzer (DMA, TSI 3081) and a Condensation

163   Particle Counter (CPC, TSI 3775). For nucleation and low AS experiments, the measured

164   aerosol size range was set to 14 to 686 nm diameter. For high AS experiments, the

165   measured aerosol size range was set to 17 to 983 nm. Prior checks were made to confirm

166   that no particles larger than 686 nm were detected in the nucleation and low AS

167   experiments. The SOA mass concentrations reported in this study were measured using

168   the SMPS. The SOA density was calculated from the ratio of the aerosol size

169   distributions measured by the HR-ToF-AMS and the SMPS during nucleation

170   experiments (DeCarlo et al., 2004; Bahreini et al., 2005).

171   **2.2. Particle wall deposition correction**

172   Particle wall deposition needs to be accounted for to determine the SOA mass

173   concentration in the chamber. Two limiting assumptions have traditionally been made

174   regarding interactions between particles deposited on the chamber walls and suspended

175   vapors when accounting for particle wall loss in the computation of SOA mass yields

176   (Weitkamp et al., 2007; Hildebrandt et al., 2009; Loza et al., 2012; Zhang et al., 2014).

177   The first case assumes that particles deposited on the walls cease to interact with

178   suspended vapors, and therefore the SOA mass present on these deposited particles does

179   not change after deposition (Loza et al., 2012; Zhang et al., 2014). Adding the SOA mass

180   present on these deposited particles to that present on the suspended particles provides a

181   lower bound of the total SOA mass concentration. In the second case, it is assumed that

182   particles deposited on the walls continue to interact with suspended vapors as if these

183   particles had remained suspended, and therefore the SOA mass present on these

184 deposited particles increases at the same rate as those suspended (Hildebrandt et al.,

185 2009; Weitkamp et al., 2007). Thus, this case provides an upper bound of the total SOA

186 mass concentration due to the additional uptake of suspended vapors to wall-deposited

187 particles. However, it must be kept in mind that the calculated SOA mass concentration

188 can be underestimated even in the upper bound case since the calculation accounts

189 neither for differences in the vapor-particle and vapor-wall interaction and transport

190 timescales nor for the significantly larger amount of absorbing mass of the chamber walls

191 (relative to the deposited particles) for suspended vapors (McVay et al., 2014; Zhang et

192 al., 2014; McVay et al., 2016).

193   In this study, we calculate SOA mass yields using the lower bound of the total

194 SOA mass concentration obtained from SMPS measurements, which has been described

195 in detail previously (Loza et al., 2012), and will be reviewed briefly here. For each

196 particle size bin i at each time increment Δt, the particle number distribution deposited on

197 the wall ($n_{w,i,j}$) is:

198
$$n_{w,i,j} = n_{s,i,j} \times (1 - \exp(-\beta_i \Delta t)) \qquad (1)$$

199 where $n_{s,i,j}$ is the suspended particle number distribution in particle size bin i at time step

200 j, Δt is the difference between time step j and time step $j + 1$, and β_i is the size-dependent

201 first-order exponential wall loss rate obtained from seed-only experiments. The particle

202 wall loss corrected number distribution ($n_{total,i,j}$) is obtained from the sum of the particle

203 number distribution of deposited particles ($n_{w,i,j}$) and suspended particles ($n_{s,i,j}$):

204
$$n_{total,i,j} = n_{s,i,j} + n_{w,i,j} \qquad (2)$$

205 Assuming spherical particles, the particle wall loss corrected volume concentration

206 ($V_{total,j}$) is:

207
$$V_{total,j} = \sum_{i=1}^{m} \frac{n_{total,i,j}}{D_{p,i} \ln 10} \times (D_{p,i+} - D_{p,i-}) \times \frac{\pi}{6} D_{p,i}^3 \qquad (3)$$

208 where m is the number of particle size bins, $D_{p,i+}$ and $D_{p,i-}$ are the upper and lower limits

209 for size bin i, respectively, and $D_{p,i}$ is the median particle diameter for size bin i. The term

210     $D_{p,i}\ln 10$ is needed to convert from a lognormal distribution. Figures S1-S4 and Table S1

211   show results from the particle wall loss correction. To calculate the SOA mass

212   concentration ($\Delta M_{o,j}$), the SOA density (ρ_{org}) is multiplied by the difference of the

213   particle wall loss corrected volume concentration ($V_{total,j}$) and the initial seed volume

214   concentration (V_{seed}):

215
$$\Delta M_{o,j} = \rho_{org} \times (V_{total,j} - V_{seed}) \tag{4}$$

216   The measured densities of the α-pinene SOA are 1.39 and 1.37 g cm^{-3} for the 100 and 500

217   ppb O$_3$ experiments, respectively, and are within the range (i.e., 1.19 to 1.52 g cm^{-3})

218   reported in previous α-pinene ozonolysis studies (Bahreini et al., 2005; Kostenidou et al.,

219   2007; Song et al., 2007; Shilling et al., 2009).

220   **3. Vapor-particle dynamics model**

221   A coupled vapor-particle dynamics model is used to evaluate the influence of seed

222   aerosol surface area and oxidation rate on SOA formation in the α-pinene ozonolysis

223   chamber experiments. This model is similar to that used in McVay et al. (2014), and will

224   be briefly described here. Parameters from the experimental data (temperature, pressure,

225   initial α-pinene concentration) are used as model inputs. The initial size distribution is set

226   to that measured by the SMPS, with the exception of the two nucleation experiments.

227   Because nucleation is not explicitly simulated, an approximation is used in which the

228   smallest diameter bin is initialized with the total number of particles measured at the end

229   of the experiment (see Table S1). In each simulation, the decay of α-pinene, the

230   consumption of O$_3$, the SOA mass concentration, and the SOA mass yield are calculated

231   throughout the duration of the experiment. We assume a linear injection rate of O$_3$ based

232   on the time required to inject the desired O$_3$ concentration. For example, O$_3$ is injected at

233   a rate of 500/54.25 ppb min^{-1} for the first 54.25 min during the 500 ppb O$_3$ experiments.

234   O$_3$ simultaneously decays by reaction with α-pinene at a rate constant of 9.4×10^{-17} cm^3

235   molec.$^{-1}$ s^{-1} (Saunders et al., 2003). The O$_3$+α-pinene reaction is assumed to occur in a

236   well-mixed chamber and produces 5 classes of first-generation products, which are

237   grouped according to mass saturation concentrations, similar to the volatility basis set

238   (Donahue et al., 2006): >10^3 (assumed to be completely volatile), 10^2, 10, 1 and 0.1 µg

239   m^{-3}. Branching ratios between these products are optimized to fit the experimental data.

240   These branching ratios cannot be compared directly to previously reported VBS

241   parameters for α-pinene ozonolysis (e.g., Henry et al. (2012)) since VBS parameters are

242   typically mass-based, while the branching ratios in the model are mole-based.

243   Furthermore, the branching ratios here account for the influence of vapor wall deposition,

244   while typical VBS parameters do not. We assume that these 5 classes of products have

245   molecular weights 168, 184, 192, 200 and 216 g mole^{-1} based on the group contribution

246   method (Donahue et al., 2011). The first-generation products are assumed not to undergo

247   further reaction with O$_3$ upon formation.

248   The aerosol dynamics in the chamber obey the aerosol general dynamic equation

249   (Seinfeld and Pandis, 2006):

$$\left(\frac{\partial n(D_p,t)}{\partial t}\right) = \left(\frac{\partial n(D_p,t)}{\partial t}\right)_{coag} + \left(\frac{\partial n(D_p,t)}{\partial t}\right)_{cond/evap} + \left(\frac{\partial n(D_p,t)}{\partial t}\right)_{wall\ loss} \tag{5}$$

251   Coagulation is not considered, since an alternative version of the model including

252   coagulation showed no change in the predicted α-pinene ozonolysis SOA mass

253   concentrations in simulations with and without coagulation. The change in particle

254   number distribution due to particle wall loss is:

$$\left(\frac{\partial n(D_p,t)}{\partial t}\right)_{wall\ loss} = -\beta_j(D_p)n(D_p,t) \tag{6}$$

256   where, as noted in section 2.2, $\beta_j(D_p)$ is the size-dependent first-order wall loss rate

257   coefficient obtained from fitting seed-only experiments. The rate at which vapor

258   condenses onto a spherical aerosol particle is:

$$J_i = 2\pi D_p D_i (G_i - G_i^{eq}) F_{FS} \tag{7}$$

260   where G_i is the concentration of gas-phase species i, G_i^{eq} is the saturation concentration

261   of gas-phase species i, D_i is the gas-phase molecular diffusivity (assumed to be 3×10^{-6}

262   m^2 s^{-1} (McVay et al., 2014)), and F_{FS} is the Fuchs-Sutugin correction for non-continuum

263   gas-phase diffusion:

264
$$F_{FS} = \frac{0.75\alpha_p(1+\text{Kn})}{\text{Kn}^2 + \text{Kn} + 0.283\text{Kn}\alpha_p + 0.75\alpha_p}$$
(8)

265   where α_p is the vapor-particle mass accommodation coefficient, and Kn is the Knudsen

266   number, Kn = $2\lambda_{AB}/D_p$. The vapor-particle mass accommodation coefficient accounts for

267   any resistance to vapor molecule uptake at the particle surface (e.g. surface

268   accommodation and particle-phase diffusion limitations). λ_{AB} is the mean free path of the

269   gas-phase species, which is:

270
$$\lambda_{AB} = 3D_i \times \sqrt{\frac{\pi M_i}{8RT}}$$
(9)

271   where R is the ideal gas constant, T is the temperature, and M_i is the molecular weight of

272   diffusing gas-phase molecule i. For each particle size bin, Eqs. 7-9 are used to compute

273   the flux of each gas-phase species to and from an aerosol particle, scaled by the particle

274   number concentration in the size bin. The net rate of change for each gas-phase species

275   due to evaporation or condensation is obtained from the total flux summed over all the

276   particle size bins.

277   G_i^{eq} varies for each particle size bin because it depends on the mass concentration

278   of species i and the total organic mass concentration in the size bin:

279
$$G_i^{eq} = \frac{A_i C_i^*}{\sum\limits_k A_k + M_{init}}$$
(10)

280   where A_i is the concentration of species i in the particle phase, C_i^* is the saturation

281   concentration of species i, $\sum\limits_k A_k$ is the sum of all the species concentration in the particle

282   phase, and M_{init} is the mass concentration of any absorbing organic material initially

283 present in the seed aerosol. To avoid numerical errors in Eq. 10 at the first time step, M_{init}

284 is set to 0.01 µg m^{-3}.

285   The oxidation products of α-pinene ozonolysis are assumed to be subject to

286 vapor-wall deposition, which is simulated using a first-order wall-loss coefficient

287 (McMurry and Grosjean, 1985):

288
$$k_{wall,on} = (\frac{A}{V})\frac{\frac{\alpha_{wall}\bar{c}}{4}}{1+\frac{\pi}{2}(\frac{\alpha_{wall}\bar{c}}{4\sqrt{k_e D_i}})} \qquad (11)$$

289 where A/V is the surface area-to-volume ratio of the chamber (estimated to be 2.5 m^{-1}),

290 α_{wall} is the vapor-wall mass accommodation coefficient, and k_e is the eddy diffusion

291 coefficient that describes mixing conditions in the chamber. Based on the measured size-

292 dependent particle wall loss rates (method is described in Zhang et al. (2014)), k_e is

293 estimated to be 0.03 s^{-1} for the GTEC chamber. Vapor-wall deposition is assumed to be

294 reversible, and the rate constant of vapor desorption from the chamber walls is:

295
$$k_{wall,off} = \frac{k_{wall,on}}{K_W C_W} = k_{wall,on}(\frac{C_i^* M_w \gamma_w}{C_W M_p \gamma_p}) \qquad (12)$$

296 where C_w is the equivalent organic mass concentration in the wall (designated to treat

297 gas-wall partitioning in terms of gas-particle partitioning theory and not necessarily

298 representative of a physical layer of organic concentration on the wall (Matsunaga and

299 Ziemann, 2010)), K_w is the gas-wall partitioning coefficient, M_w is the effective molecular

300 weight of the wall material, γ_w is the activity coefficient of the species in the wall layer,

301 M_p is the average molecular weight of organic species in the particle, and γ_p is the activity

302 coefficient of the species in the particle. For simplicity, we assume that $M_w = M_p$ and $\gamma_w =$

303 γ_p. C_w is set to 10 mg m^{-3} based on previous inferences by Matsunaga and Ziemann

304 (2010). Sensitivity studies (not shown) show no change in model predictions when

305 varying C_w above $C_w = 0.1$ mg m^{-3}.

306   In the initial version of the model, after all the α-pinene is consumed, vapor wall

307   deposition was assumed to continue to deplete the gas-phase oxidation products and

308   aerosol mass evaporates to maintain gas-particle equilibrium. SOA evaporation was not

309   observed experimentally (i.e., the SOA mass concentration does not decrease

310   significantly over time after peak SOA growth has been achieved in these chamber

311   experiments (Fig. 2)). In order to represent these observations in the model, a first-order,

312   particle-phase reaction is introduced by which aerosol species are converted into non-

313   volatile absorbing organic mass with a timescale of τ_{olig}. This mechanism (which is not

314   included in the model used in McVay et al. (2014)) is similar to that used by the

315   sequential equilibrium partitioning model, in which aerosol is converted from an

316   absorbing to non-absorbing, non-volatile phase in order to explain the inhibited diffusion

317   and evaporation observed in α-pinene ozonolysis SOA (Cappa and Wilson, 2011).

318   Although we assume here that the converted non-volatile aerosol mass still participates in

319   partitioning, either mechanism invokes a particle-phase process to retard SOA

320   evaporation.

321   Model parameters α_w, α_p, τ_{olig} and the branching ratios between the oxidation

322   products are optimized to best-fit the predictions with the experimental observations.

323   Specifically, model predictions are compared to experimental data: SOA mass

324   concentration vs. reaction time, α-pinene concentration vs. reaction time, and O_3

325   concentration vs. reaction time. Figure S6 compares reaction profiles of measured and

326   modeled O_3 and α-pinene concentrations for the base model case. Sensitivity tests were

327   also performed on each model parameter, shown in Figs. S7-S10. Table 2 summarizes the

328   parameters used. While the optimized parameters provide a good fit to the data, we

329   caution that the parameters are interconnected, and other fits may also be possible. We

330   are confident that our conclusions derived using these parameters are robust.

331   **4. Results**

332   Figure 1 shows the size-dependent particle wall deposition coefficients inferred

333   from seed-only deposition experiments. The initial total AS seed surface area

334   concentration in the low AS-seed only and high AS-seed only experiments (which are

335   conducted using 0.015 M AS and 0.05 M AS solutions, respectively) are similar to those

336   used in the α-pinene ozonolysis experiments (i.e., ~1000 and ~3000 μm^2 cm^{-3},

337   respectively). While there are differences in the particle wall deposition coefficients from

338   the low and high AS-seed only experiments, this difference is likely the result of

339   uncertainties arising from the low particle number concentrations for the larger particles

340   in the low AS-seed only experiment. As shown in Fig. 1, both sets of particle wall

341   deposition coefficients generally fall within the range of those measured in routine

342   monthly AS-seed only experiments conducted in the chamber.

343   The particle wall deposition corrected number concentration data provide a test of

344   the appropriateness of the particle wall deposition correction. This is because the

345   corrected number concentration should level off at a constant value (i.e., the initial

346   particle number concentration), assuming no significant coagulation, when particle wall

347   deposition is properly accounted for since the wall-deposited particle number distribution

348   is added to the suspended particle number distribution during particle wall loss

349   correction. We account for particle wall deposition in nucleation and low AS experiments

350   using deposition coefficients determined from the low AS-seed only experiments, while

351   particle deposition in high AS experiments are accounted for using coefficients

352   determined from the high AS-seed only experiments. Figures S1 and S2 show the particle

353   wall deposition-corrected aerosol number and volume concentrations. Over all

354   experiments, the particle wall deposition-corrected final particle number concentration

355   (i.e., at the end of the reaction) is 9 to 17 % less than the initial particle number

356   concentration for the low AS and high AS experiments (Table S1), respectively,

357   indicating that the particle wall deposition-corrected volume concentrations are slightly

358   underestimated. It is currently unclear why the particle wall deposition-corrected final

359   particle number concentrations are somewhat smaller than the initial particle number

360   concentrations, though this could be due to variations in particle wall deposition rates in

361   the AS-seed only and α-pinene ozonolysis experiments. As a sensitivity test, we used the

362   average of the low AS-seed only and high AS-seed only particle wall deposition

363   coefficients to account for particle wall deposition in all the experiments (Figs. S3 and

364   S4). While there is a negligible difference in the particle wall deposition corrected

365   volume concentrations (Figs. S3 and S4 vs. Figs. S1 and S2), a larger spread (1 to 22 %)

366   exists in the difference between the initial and final particle number concentrations when

367   the average particle wall deposition coefficients are used (Table S1). Therefore, all

368   subsequent nucleation and low AS data presented here are particle wall deposition-

369   corrected using coefficients determined from the low AS-seed only experiments, and all

370   high AS data are corrected using particle wall deposition coefficients determined from

371   the high AS-seed only experiments.

372   Figure 2 shows the reaction profiles of the α-pinene ozonolysis experiments. SOA

373   growth typically starts within 10 to 20 min of the start of the reaction. At either initial O_3

374   concentration, the molar ratio of O_3 reacted to α-pinene reacted is approximately 1:1 (i.e.,

375   50 ppb α-pinene reacted with 50 ppb O_3), which indicates that O_3 reacts only with α-

376   pinene and not its oxidation products. As anticipated, the α-pinene oxidation rates in the

377   100 ppb O_3 experiments are significantly slower than those in the 500 ppb O_3

378   experiments. Figures 2a-c show that peak SOA levels are typically reached at reaction

379   time ~300 to 350 min in the 100 ppb O_3 experiments, during which ≥ 95 % of the

380   injected α-pinene has reacted. In contrast, all the α-pinene reacts within 80 to 90 min of

381   the start of reaction in the 500 ppb O_3 experiments, and peak SOA levels are achieved at

382   reaction time ~100 min (Figs. 2d-f). These results indicate that the O_3 concentration

383   dictates both the rate of α-pinene oxidation and the time it takes to achieve peak SOA

384   growth.

385   Figure 3 shows the time-dependent growth curves (SOA mass concentration vs.

386   α-pinene reacted (Ng et al., 2006)) for the 100 and 500 ppb O_3 experiments. Only SOA

387   growth data up to SOA peak concentrations are shown. SOA growth essentially stops

388   once all the α-pinene has reacted. This is expected, as α-pinene has only one double

389   bond; the first step of α-pinene ozonolysis is rate-limiting and the first-generation

390   products are condensable (Ng et al., 2006; Chan et al., 2007). The time-dependent SOA

391   growth curves for experiments corresponding to different seed aerosol concentrations

392   overlap for both low and high O_3 concentrations. This indicates that the initial AS seed

393   surface area does not influence the SOA growth rate within the range of AS seed surface

394   area concentration used. It is important to note that while it appears that the SOA growth

395   rate is faster in the 100 ppb O_3 relative to the 500 ppb O_3 experiments based on the time-

396   dependent growth curves shown in Fig. 3, this is not the case. Instead, the observed time-

397   dependent growth curves can be explained by the higher concentration of α-pinene

398   having reacted during the 10 to 20 min delay of SOA formation in the 500 ppb O_3

399   experiments compared to the 100 ppb O_3 experiments (Fig. 2).

400   Figure 4 shows the time-dependent SOA mass yields as a function of initial total

401   AS seed surface area for the 100 and 500 ppb O_3 experiments. Regardless of the O_3

402   concentration, the SOA mass yields stay roughly constant despite the increase in AS seed

403   surface area. This indicates that the surface area concentration of AS seed aerosol does

404   not noticeably influence the partitioning of gas-phase α-pinene ozonolysis products to the

405   particle phase within the range of AS seed surface area concentration used. Higher SOA

406   mass yields are observed in the 500 ppb O_3 experiments, which indicates that the α-

407   pinene oxidation rate controls the absolute amount of SOA formed. It is important to note

408   that these conclusions are robust even when the average of the low AS-seed only and

409   high AS-seed only particle wall loss coefficients are used to account for particle wall loss

410   in all the experiments (Fig. S5). The enhancement of SOA mass yields at higher O_3

411   concentrations and the lack of a SOA mass yield dependence on AS seed surface area

412   (within the range of AS seed surface area concentration used in this study) will be

413   discussed further in Section 5.

414   The α-pinene ozonolysis SOA mass yields obtained in this study are compared to

415   those reported in previous studies in Fig. 5. Table S2 lists the experimental conditions

416   employed in these studies. To facilitate comparison between the different studies, all the

417   SOA mass yield and concentration data (including this study) are adjusted to an organic

418   density of 1.0 g cm^{-3}. As shown in Fig. 5, the SOA mass yields obtained at peak SOA

419   growth in this study are generally consistent with those of previous studies where the

420   chamber was operated in batch mode (that in this study).

421   The competition between the condensation of SOA-forming vapor to aerosol

422   particles vs. to chamber walls is investigated using the coupled vapor-particle dynamics

423   model described in Section 3. As noted earlier, optimal model values for α_p, α_w, τ_{olig} and

424   the branching ratios between the oxidation products were determined for the 100 and 500

425   ppb O_3 experiments by comparing the observed and best-fit time-dependent SOA, α-

426   pinene, and O_3 concentrations profiles (Figs. S6-S10). Sensitivity tests were performed

427   for each parameter to establish that the set of optimal model values provide the best

428   overall agreement with time-dependent SOA formation profiles observed for all

429   experiments (Figs. S7-S10). Predictions from the coupled vapor-particle dynamics model

430   show that the optimal parameters are: $\alpha_w = 10^{-6}$, $\alpha_p = 1$, $\tau_{olig} = 4$ h, branching ratios = 0.57,

431   0.35, 0.04, 0.015 and 0.025 for oxidation products with vapor pressures $>10^3$, 10^2, 10, 1

432   and 0.1 $\mu g\ m^{-3}$, respectively. The best-fit $\alpha_w = 10^{-6}$ (Fig. S7) corresponds to a first-order

433   vapor-wall deposition rate constant ($k_{wall,on}$) of 10^{-4} s^{-1}. This $k_{wall,on}$ value is comparable to

434   that reported by Matsunaga and Ziemann (2010) for a 8.2 m^3 chamber.

5. Discussion

436   α-pinene ozonolysis has been carried out at two O_3 mixing ratios (100 and 500

437   ppb) under varying AS seed aerosol surface area concentrations (0, ~1000 and ~3000 μm^2

438   cm^{-3}).

5.1 Seed aerosol surface area effect

440   Figure 3 shows that the time-dependent SOA growth curves for experiments with

441   different seed area concentrations overlap at both O_3 concentrations, which indicates the

442   AS seed surface area does not affect the rate of SOA growth within the range of AS seed

443   surface area concentration used in this study. This observation differs from findings by

444   Pathak et al. (2007b) for the O_3+α-pinene system, who showed that even though the final

445   SOA mass yields measured in the reaction of 7.3 ppb α-pinene with 1500 ppb O_3 were

446   similar in their seeded and unseeded experiments, SOA growth was considerably slower

447   in unseeded experiments compared to seeded experiments. The authors suggested that the

448   slow SOA formation rate in their unseeded experiment was the result of SOA formation

449   being limited by the mass transfer of semi-volatile oxidation products to newly formed

450   particles (via nucleation) during the early stages of the experiment. These newly formed

451   particles have a significantly smaller aerosol surface area for gas-particle partitioning as

452   compared to that of seed aerosol particles in the seeded experiments. Consequently, the

453   semi-volatile oxidation products accumulated in the gas phase during the early stages of

454   the unseeded experiments, resulting in slower SOA growth compared to the seeded

455   experiments. The observation that the presence of seed aerosol does not influence the

456   SOA growth rate in the present study may be explained by the relatively high

457   concentrations of α-pinene reacted and SOA mass loadings obtained. Previous studies

458   have shown that the delay between the onset of VOC oxidation and SOA formation in

459   unseeded experiments is most pronounced at low aerosol loadings (Kroll et al., 2007).

460   We note that the concentrations of α-pinene reacted and SOA mass loadings obtained in

461   this study are significantly larger than those reported by Pathak et al. (2007b). Therefore,

462   it is possible that due to the relatively large concentrations of α-pinene reacted in this

463   study, substantial concentrations of gas-phase oxidation products are generated, which

464   results in rapid partitioning into the particle phase even in the absence of seed aerosol.

465   This is evident from the large increase in the particle number concentration during the

466   early stages of the unseeded 100 and 500 ppb O_3 experiments, where the particle number

467   concentration increased to ~8000 and ~10000 particles/cm^3 during the first 45 min of the

468   100 and 500 ppb O_3 experiments, respectively (Fig. S1a and S2a). Thus, the SOA growth

469   rates are not controlled by the presence of AS seed in this study.

470   Figure 4 shows that for both initial O_3 mixing ratios used, the time-dependent

471   SOA mass yield is similar at any given AS seed surface area (see also Table 1). The

472   absence of a SOA growth dependence on the AS seed surface area is similar to

473   observations reported by McVay et al. (2016) for the α-pinene photooxidation (OH-

474   driven chemistry) system, but differ from those reported by Zhang et al. (2014) for the

475   toluene photooxidation system in which the SOA mass yield increased with the surface

476   area concentration of seed aerosol.

477   The best-fit $\alpha_p = 1$ (Fig. S8) suggests the absence of significant limitations to

478   vapor-particle mass transfer in the present α-pinene ozonolysis study, and that SOA

479   formation is governed by quasi-equilibrium growth (McVay et al., 2014), which occurs

480   when SOA-forming vapors are produced at a rate that is significantly slower than that

481   required to establish gas-particle equilibrium (Shiraiwa and Seinfeld, 2012; Zhang et al.,

482   2012). Moreover, the characteristic timescale to establish gas-particle equilibrium is less

483   than those for reaction and vapor-wall deposition. When the vapor and particle phases

484   maintain equilibrium, gas-particle equilibrium is controlled by the amount of organic

485   matter in the VOC system. As a result, the rate of condensation of SOA-forming vapors

486   is independent of the seed aerosol surface area (McVay et al., 2014). The best-fit $\alpha_p = 1$ is

487   within the approximate range of α_p coefficients determined from α-pinene ozonolysis

488   SOA thermodenuder studies ($\alpha_p = 0.1$) (Saleh et al., 2013) and α-pinene photooxidation

489   chamber studies ($\alpha_p = 0.1$ or 1) (McVay et al., 2016). Notably, this result differs markedly

490   from that for toluene photooxidation (Zhang et al., 2014), where α_p was determined to be

491   0.001, and for which, since the SOA mass yield was strongly dependent on the seed

492   aerosol surface area, the condensation of SOA-forming vapors onto seed aerosol particles

493   was kinetically limited (McVay et al., 2014). Kinetically-limited SOA growth occurs

494   when the timescale for gas-particle equilibrium is competitive with or exceeds the

495   timescale for reaction and vapor wall deposition, and may reflect imperfect

496   accommodation of gas-phase organics to the particle phase. The markedly different

497   behavior of the α-pinene and toluene SOA systems could be due to differences in SOA

498   volatility and aerosol physical phase state (McVay et al., 2016).

499   **5.2 Oxidation rate effect**

500   At higher O_3 concentrations, the α-pinene oxidation rate increases, leading to

501   higher SOA mass yields (the "oxidation rate effect"). This behavior was previously

502   observed by Ng et al. (2007) for the *m*-xylene photooxidation system, for which the

503   oxidation rate effect was attributed to the loss of semi-volatile condensable products to

504   chamber walls in competition with condensation onto seed particles to form SOA.

505   SOA formation from α-pinene ozonolysis is presumed to be driven by a range of

506   semi- and low-volatility first-generation products arising from reaction of O_3 with the

507   single C=C double bond (Ng et al., 2006). These products are subject to two competing

508   routes: condensation to particles to form SOA or deposition on the chamber walls. Each

509   process can be represented in terms of a first-order rate constant: $k_{wall,on}$ and $k_{particle,on}$ (s^{-1}).

510   The rate of vapor-wall deposition of condensable species A is then $k_{wall,on} \times$ [A] (molec

511    $cm^{-3} s^{-1}$) and the rate of condensation onto particles is $k_{particle,on} \times$ [A] (molec $cm^{-3} s^{-1}$).

512   Increasing the rate of reaction increases the concentration of [A], but the relative rates of

513   vapor-wall deposition and condensation onto particles will remain the same. In general,

514   however, both vapor-wall deposition and vapor-particle condensation are reversible

515   processes (McVay et al., 2014; Zhang et al., 2014). The first-order rate constant for

516   evaporation from the wall can be represented as (Matsunaga and Ziemann, 2010):

517
$$k_{wall,off} = k_{wall,on} \left(\frac{C_i^*}{C_w} \right)$$
(13)

518   where C_i^* is the saturation concentration and C_w is the assumed equivalent wall organic

519   concentration. The rate of evaporation from particles is:

520
$$k_{particle,off} = k_{particle,on} \left(\frac{C_i^*}{C_{aer}} \right)$$
(14)

521   where C_{aer} is the organic aerosol concentration ($C_{aer} = \Sigma A_k + M_{init}$).

522   The difference between C_{aer} and C_w is the key to explaining the oxidation rate

523   effect. At the beginning of the experiment, C_{aer} is very small because the inorganic seeds

524   are essentially non-absorbing. Therefore, $k_{particle,off}$ is large, and the net SOA growth is

525   small. In contrast, C_w is considered to be substantial (on the order of 10 mg m^{-3}) and to be

526   essentially constant throughout the experiment (Matsunaga and Ziemann, 2010; McVay

527   et al., 2014; Zhang et al., 2014). Model predictions are insensitive to the value of C_w

528   since, in any event, C_w is significantly larger than C_{aer} (Zhang et al., 2014). Therefore,

529    $k_{wall,off}$ is small at the beginning of the experiment and the net vapor wall loss rate is fast.

530   As C_{aer} increases, the net SOA condensation rate increases relative to the net vapor wall

531   loss rate. When the reaction rate increases corresponding to higher O$_3$ concentrations, C_{aer}

532   grows more quickly because more condensable species are available to form SOA, and

533   the net condensation rate increases more rapidly. Therefore, the observed oxidation rate

534   effect is due to vapor wall deposition, and arises because vapor-particle and vapor-wall

535   condensation are essentially reversible processes. This explanation is consistent with

536   simulations varying the O$_3$ concentration in which all species are non-volatile (i.e., do not

537   evaporate from the particles or the wall). In this case, no oxidation rate effect is observed

538   as the O$_3$ concentration increases. The growth curves for different O$_3$ concentrations

539   overlap, and the same yield is obtained regardless of O$_3$ concentration (Fig. S11).

540   Sensitivity tests were performed to determine the point at which SOA formation is

541   no longer influenced by the O_3 concentration. In these simulations, the initial α-pinene

542   concentration is fixed at 48 ppb, while the O_3 concentration is varied from 75 to 1000

543   ppb. The rate of O_3 injection is assumed to remain constant as the O_3 concentration is

544   increased to mimic the experimental protocol (i.e., O_3 injection time is increased to

545   achieve higher O_3 concentrations). The O_3 injection rate used in these simulations is fixed

546   at $500/54.25$ ppb min^{-1}, which is the same as that used to analyze results from the 500

547   ppb O_3 experiments. Model predictions in Fig. S12 show that the maximum SOA mass

548   concentration increases with increasing O_3 concentration up to approximately 500 ppb

549   O_3. Beyond this O_3 concentration, the SOA growth curves overlap and the maximum

550   SOA mass concentration does not increase even when more O_3 is added. This plateau

551   arises due to the lengthening time required to inject increasing amounts of O_3. More than

552   1 h is required to inject > 500 ppb of O_3, and by this time, virtually all of the α-pinene has

553   reacted. Increasing the O_3 concentration after all of the α-pinene has reacted does not lead

554   to any changes in the SOA mass concentration. However, if a faster injection rate of O_3 is

555   used, the oxidation rate effect will persist to higher O_3 concentrations (i.e., > 500 ppb O_3)

556   (Fig S13). With a faster injection rate, 500 ppb O_3 is injected before all of the α-pinene

557   has reacted. Continuing to inject O_3 to a higher concentration (i.e., 750 ppb) will cause α-

558   pinene to decay faster and SOA to grow faster than when the O_3 injection stops at 500

559   ppb. The oxidation rate effect is then apparent at higher O_3 concentrations. If, instead of

560   using an injection rate of O_3, simulations are run using fixed initial O_3 (not possible

561   experimentally), the rate effect persists to even higher O_3 concentrations. The relative

562   increase in yield with increasing O_3 concentrations slows at very high O_3 concentrations

563   because the rate of reaction becomes substantially faster than the vapor wall deposition

564   rate, and there is less marginal effect to increasing the reaction rate.

565   **5.3 Interplay of the seed aerosol surface area effect and the oxidation rate effect**

566   In this study, we observe an oxidation rate effect but not a seed aerosol surface

567   area effect. In Zhang et al. (2014), a seed aerosol surface area effect was observed, but

568   the variation of the oxidation rate was not studied. A key aspect of vapor wall deposition

569   is the potential interplay between the seed aerosol surface area effect and the oxidation

570 rate effect. To examine this interplay in the α-pinene ozonolysis system, simulations were

571 carried out by varying the seed aerosol surface area and the O_3 concentration

572 simultaneously, while using the branching ratios, oligomerization rate, and vapor wall

573 deposition rate parameters obtained in the present study. The initial α-pinene

574 concentration was set to 50 ppb, and a fixed O_3 concentration was used in place of a

575 linear injection. α_p was varied at 0.001, 0.01, and 1 in these simulations. Figure 6 shows

576 the SOA mass yield at peak SOA growth as a function of both the seed aerosol surface

577 area and O_3 concentration for $\alpha_p = 1$, 0.01, and 0.001. For $\alpha_p = 1$, the oxidation rate

578 dominates: SOA mass yield increases significantly as O_3 concentration increases while

579 the seed aerosol surface area has a negligible effect. For $\alpha_p = 0.01$, both effects can be

580 observed in different regions: at low O_3 concentrations and high seed aerosol surface

581 areas, the oxidation rate effect dominates; at low seed aerosol surface areas and high O_3

582 concentrations, the seed surface area dominates. At low seed aerosol surface areas and

583 low O_3 concentrations, both effects are present. For $\alpha_p = 0.001$, the seed aerosol surface

584 area effect dominates except at very high seed aerosol surface areas. These observations

585 show that the presence of an oxidation rate effect and/or seed aerosol surface area effect

586 depends on a complex interplay of factors, such as α_p, the rate of hydrocarbon oxidation,

587 and the amount of seed surface area present.

588 **6. Implications**

589   In this study, we systematically examine the roles of gas-particle partitioning and

590 VOC oxidation rate in the presence of vapor-wall deposition in α-pinene ozonolysis. We

591 show that despite the presence of vapor-wall deposition, SOA mass yields at peak SOA

592 growth remain approximately constant regardless the seed aerosol surface area (within

593 the range of AS seed surface area concentration used in this study). This observation is

594 consistent with SOA formation in the α-pinene ozonolysis system being governed by

595 quasi-equilibrium growth, for which there are no substantial limitations to vapor-particle

596 mass transfer. This result was demonstrated in a previous modeling study which showed

597 that increasing the seed-to-chamber surface area ratio will lead to increased SOA growth

598 only in cases in which the condensation of SOA-forming vapors onto seed aerosol

599   particles is kinetically limited as a result of imperfect accommodation of gas-phase

600   organics to the particle phase (McVay et al., 2014).

601   An important implication of this study is that diverting vapor-wall deposition in

602   chamber studies via the addition of ever-increasing quantities of seed aerosol particles is

603   not effective in VOC systems for which SOA formation is governed by quasi-equilibrium

604   growth. This study also underscores the importance of accounting for particle wall

605   deposition appropriately in chamber studies, to avoid erroneous conclusions regarding the

606   role of gas-particle partitioning (quasi-equilibrium vs. kinetically-limited SOA growth) in

607   influencing vapor wall loss in the VOC system.

608   We note that the present study shows that the SOA mass yield is independent of

609   seed aerosol surface area concentration for values ranging from 0 to ~3000 μm^2 cm^{-3}.

610   This corresponds to a seed-to-chamber surface area ratio of 0 to ~1 × 10^{-3}, which is

611   substantially smaller than the range used by Zhang et al. (2014) to study the influence of

612   vapor-wall deposition on toluene photooxidation SOA formation in the Caltech chamber

613   (i.e., 0 to ~5 × 10^{-3}). It is possible that a SOA mass yield dependence on the seed surface

614   area may have become more apparent had a larger range of seed aerosol surface area (i.e.,

615   > 3000 μm^2 cm^{-3}), and hence a larger range of seed-to-chamber surface area ratio, been

616   used here. One consideration is that coagulation may become increasingly important, and

617   will need to be accounted for, when higher seed aerosol number concentrations (relative

618   to those used in this study) are used (Seinfeld and Pandis, 2006; Pierce et al., 2008). A

619   detailed analysis of the effect of seed aerosol surface area concentrations > 3000 μm^2 cm^{-}

620   ^{3} on α-pinene ozonolysis SOA mass yields will be the subject of forthcoming work.

621   Higher SOA mass yields at peak SOA growth are observed in the present study

622   when O_3 is increased from 100 to 500 ppb. This is because α-pinene is oxidized more

623   quickly, which leads to gas-phase oxidation products being formed more rapidly, and

624   consequently partitioning more quickly onto AS seed aerosol particles before they are

625   lost to the chamber walls. Therefore, the oxidation rate effect (i.e., higher SOA mass

626   yields as a result of faster hydrocarbon oxidation rates) is a consequence of vapor-wall

627   deposition. An important implication of this study is that SOA mass yields can be

628   affected by vapor-wall deposition in VOC systems that are not characterized by slow

629   mass accommodation of gas-phase organics to the particle phase (Zhang et al., 2014).

630   Thus, this work demonstrates that the effect of vapor-wall deposition on SOA mass yields

631   can be mitigated through the use of excess oxidant concentrations. It should be noted that

632   the α-pinene ozonolysis SOA mass yields (absolute values) increased by 5 to 9 % when

633   O_3 is increased from 100 to 500 ppb (for an initial α-pinene concentration of ~50 ppb),

634   where SOA formation is governed by quasi-equilibrium growth. In the absence of vapor-

635   wall deposition, SOA mass yields are predicted by the model used here to approximately

636   double from those observed experimentally. In contrast, Zhang et al. (2014) showed that

637   the presence of vapor-wall deposition led to underestimation of SOA formation by factors

638   as much as four in the toluene photooxidation system, where the condensation of SOA-

639   forming vapors onto seed aerosol is kinetically limited. Taken together, these results

640   indicate that the magnitude by which vapor-wall deposition affects SOA mass yields

641   depends on the extent to which the VOC system is governed by kinetically-limited SOA

642   condensational growth.

643   Given these observations of how gas-particle partitioning can influence the

644   magnitude by which vapor-wall deposition affects SOA mass yields, an overriding

645   question is: what controls the gas-particle partitioning behavior of SOA formed in

646   different VOC systems? α_p describes the overall mass transfer of vapor molecules into the

647   particle phase (McVay et al., 2014; Zhang et al., 2014). Thus, α_p affects the vapor-

648   particle equilibrium timescale, which, depending on the extent to which it is competitive

649   with the timescales for reaction and vapor-wall deposition, determines whether SOA

650   formation is governed by kinetically-limited or quasi-equilibrium growth. Markedly

651   different α_p values could arise from the physical phase state of the SOA formed. As

652   discussed by McVay et al. (2014, 2016), if the SOA formed exists in a semi-solid state

653   (Vaden et al., 2010; Virtanen et al., 2010; Cappa and Wilson, 2011; Vaden et al., 2011;

654   Virtanen et al., 2011; Kuwata and Martin, 2012; Perraud et al., 2012; Saukko et al., 2012;

655   Abramson et al., 2013; Renbaum-Wolff et al., 2013), a low value of α_p might be expected

656   owing to retarded surface accommodation and particle-phase diffusion (Zaveri et al.,

657   2014). Quantification of α_p is challenging experimentally, and reported α_p values for the

658   same system can vary by several orders of magnitude (Grieshop et al., 2007; Stanier et

659   al., 2007; Vaden et al., 2011; Miles et al., 2012; Saleh et al., 2013). Therefore, α_p of SOA

660 formed in different VOC systems need to be better constrained through a combination of

661 experimental and modeling efforts.

662 The SOA mass yield from the ozonolysis of monoterpenes in the GEOS-CHEM

663 chemical transport model (19 % at 10 μg m^{-3}) is currently based on that measured in α-

664 pinene ozonolysis studies by Shilling et al. (2008) (Pye et al., 2010). Shilling et al. (2008)

665 measured these SOA mass yields in a teflon chamber operated in continuous-flow mode,

666 as opposed to batch mode, which is how experiments in the present study and most of

667 those shown in Fig. 5 and Table S2 were conducted. While it is not possible to directly

668 compare our results with those of Shilling et al. (2008) due to differences in SOA mass

669 concentrations, the SOA mass concentrations and yields measured in the current study

670 are generally consistent with those of previous batch chamber studies. The SOA mass

671 yields at ~10 μg m^{-3} SOA mass concentration measured by Shilling et al. (2008) are

672 generally higher than those measured in chambers operated in batch mode (Griffin et al.,

673 1999; Cocker et al., 2001b; Presto et al., 2005; Presto and Donahue, 2006; Pathak et al.,

674 2007b) (Fig. 5). One possible explanation for the higher SOA mass yields in the

675 continuous-flow, steady state, mode is that the SOA-forming vapors are in equilibrium

676 with the organic mass present on the chamber walls and seed aerosol, hence minimizing

677 the irreversible loss of SOA-forming vapors to the chamber walls (Shilling et al., 2008).

678 However, the extent to which SOA mass yields obtained in a continuous-flow reactor are

679 influenced by vapor wall loss is unclear. Using a continuous-flow reactor, Ehn et al.

680 (2014) observed α-pinene ozonolysis SOA mass yields to increase with increasing seed

681 aerosol surface area but required $\alpha_p = 1$ to fit the observed SOA growth. The observed

682 vapor-wall deposition rate constant in their continuous-flow reactor (0.011 s^{-1}) is two

683 orders of magnitude larger than that of the GTEC chamber (10^{-4} s^{-1}). The estimated

684 timescales for gas-particle and gas-wall partitioning are also approximately equal in their

685 continuous-flow reactor. This indicates that SOA condensational growth is kinetically

686 limited in their continuous-flow reactor even at $\alpha_p = 1$ (Ehn et al., 2014; McVay et al.,

687 2014), which suggests that SOA mass yields measured in their continuous-flow reactor

688 may be significantly affected by vapor-wall deposition.

689   Previous studies on SOA formation from the OH and NO_3 oxidation of biogenic

690   VOCs have similarly reported higher SOA mass yields in the presence of higher oxidant

691   concentrations. For example, in the NO_3 oxidation of β-pinene, Boyd et al. (2015)

692   reported SOA mass yields 10 to 30 % higher than those previously reported by Fry et al.

693   (2009, 2014). In addition to differences in the experimental conditions of the two studies,

694   Boyd et al. (2015) hypothesized that the higher SOA mass yields could also be a result of

695   the higher NO_3 concentrations used in their study (which led to faster β-pinene oxidation

696   rates) compared to those used by Fry et al. (2009, 2014). The oxidation rate effect was

697   also observed in the *m*-xylene photooxidation system, where Ng et al. (2007) showed that

698   the SOA mass yields were dependent on the *m*-xylene oxidation rate, with higher OH

699   concentrations (and hence faster oxidation rates) resulting in higher SOA mass yields

700   Together, these studies show that faster hydrocarbon oxidation rates can alleviate the

701   effects of vapor-wall deposition on SOA mass yields in different VOC systems.

702   This gives rise to the question: should chamber SOA experiments on different

703   VOC systems be performed under as rapid oxidation conditions as possible (i.e., large

704   oxidant concentrations) to reduce the effects of vapor-wall deposition? A recent study by

705   McVay et al. (2016) reported similar SOA growth under low and high OH levels for α-

706   pinene photooxidation. The authors hypothesized that the autoxidation mechanism likely

707   becomes a more important pathway at low OH levels (Crounse et al., 2013), and thus

708   contributes substantially to SOA growth. Therefore, it is possible that certain reaction

709   pathways and mechanisms (which are important in the atmosphere) are biased when

710   unusually high levels of oxidants are used in chamber experiments (e.g. autoxidation).

711   Thus, this underscores the need to design chamber experiments that simultaneously

712   mitigate the magnitude of vapor-wall deposition while ensuring that reaction conditions,

713   and consequently reaction pathways and oxidation products, are atmospherically relevant.

714   **Acknowledgements**

715   This research was funded by NSF Grants 1455588 and AGS-1523500, and US

716   Environmental Protection Agency STAR grant (Early Career) RD-83540301. This

717   publication's contents are solely the responsibility of the grantee and do not necessarily

718   represent the official views of the US EPA. Further, US EPA does not endorse the

719   purchase of any commercial products or services mentioned in the publication. R.C.

720   McVay was supported by a National Science Foundation Graduate Research Fellowship

721   under Grant No. DGE-1144469.

722   **References**

723   Abramson, E., Imre, D., Beranek, J., Wilson, J., and Zelenyuk, A.: Experimental

724   determination of chemical diffusion within secondary organic aerosol particles, Phys.

725   Chem. Chem. Phys., 15, 2983-2991, 10.1039/c2cp44013j, 2013.

726   Bahreini, R., Keywood, M. D., Ng, N. L., Varutbangkul, V., Gao, S., Flagan, R. C.,

727   Seinfeld, J. H., Worsnop, D. R., and Jimenez, J. L.: Measurements of Secondary Organic

728   Aerosol from Oxidation of Cycloalkenes, Terpenes, and m-Xylene Using an Aerodyne

729   Aerosol Mass Spectrometer, Environmental Science & Technology, 39, 5674-5688,

730   10.1021/es048061a, 2005.

731   Boyd, C. M., Sanchez, J., Xu, L., Eugene, A. J., Nah, T., Tuet, W. Y., Guzman, M. I., and

732   Ng, N. L.: Secondary organic aerosol formation from the β-pinene+NO3 system: effect of

733   humidity and peroxy radical fate, Atmos. Chem. Phys., 15, 7497-7522, 10.5194/acp-15-

734   7497-2015, 2015.

735   Canagaratna, M. R., Jimenez, J. L., Kroll, J. H., Chen, Q., Kessler, S. H., Massoli, P.,

736   Hildebrandt Ruiz, L., Fortner, E., Williams, L. R., Wilson, K. R., Surratt, J. D., Donahue,

737   N. M., Jayne, J. T., and Worsnop, D. R.: Elemental ratio measurements of organic

738   compounds using aerosol mass spectrometry: characterization, improved calibration, and

739   implications, Atmos. Chem. Phys., 15, 253-272, 10.5194/acp-15-253-2015, 2015.

740   Capouet, M., Müller, J. F., Ceulemans, K., Compernolle, S., Vereecken, L., and Peeters,

741   J.: Modeling aerosol formation in alpha-pinene photo-oxidation experiments, Journal of

742   Geophysical Research: Atmospheres, 113, n/a-n/a, 10.1029/2007JD008995, 2008.

743   Cappa, C. D., and Wilson, K. R.: Evolution of organic aerosol mass spectra upon heating:

744   implications for OA phase and partitioning behavior, Atmospheric Chemistry and

745   Physics, 11, 1895-1911, 10.5194/acp-11-1895-2011, 2011.

746 Cappa, C. D., Jathar, S. H., Kleeman, M. J., Docherty, K. S., Jimenez, J. L., Seinfeld, J.
747 H., and Wexler, A. S.: Simulating secondary organic aerosol in a regional air quality
748 model using the statistical oxidation model – Part 2: Assessing the influence of vapor
749 wall losses, Atmos. Chem. Phys., 16, 3041-3059, 10.5194/acp-16-3041-2016, 2016.

750 Carlton, A. G., Bhave, P. V., Napelenok, S. L., Edney, E. D., Sarwar, G., Pinder, R. W.,
751 Pouliot, G. A., and Houyoux, M.: Model Representation of Secondary Organic Aerosol in
752 CMAQv4.7, Environmental Science & Technology, 44, 8553-8560, 10.1021/es100636q,
753 2010.

754 Chan, A. W. H., Kroll, J. H., Ng, N. L., and Seinfeld, J. H.: Kinetic modeling of
755 secondary organic aerosol formation: effects of particle- and gas-phase reactions of
756 semivolatile products, Atmospheric Chemistry and Physics, 7, 4135-4147, 2007.

757 Cocker, D. R., Flagan, R. C., and Seinfeld, J. H.: State-of-the-art chamber facility for
758 studying atmospheric aerosol chemistry, Environmental Science & Technology, 35,
759 2594-2601, 10.1021/es0019169, 2001a.

760 Cocker, D. R., Clegg, S. L., Flagan, R. C., and Seinfeld, J. H.: The effect of water on gas-
761 particle partitioning of secondary organic aerosol. Part I: alpha-pinene/ozone system,
762 Atmospheric Environment, 35, 6049-6072, 10.1016/s1352-2310(01)00404-6, 2001b.

763 Crounse, J. D., Nielsen, L. B., Jorgensen, S., Kjaergaard, H. G., and Wennberg, P. O.:
764 Autoxidation of Organic Compounds in the Atmosphere, J. Phys. Chem. Lett., 4, 3513-
765 3520, 10.1021/jz4019207, 2013.

766 Crump, J. G., and Seinfeld, J. H.: Turbulent Deposition and Gravitational Sedimentation
767 of an Aerosol in a Vessel of Arbitrary Shape, Journal of Aerosol Science, 12, 405-415,
768 10.1016/0021-8502(81)90036-7, 1981.

769 DeCarlo, P. F., Slowik, J. G., Worsnop, D. R., Davidovits, P., and Jimenez, J. L.: Particle
770 morphology and density characterization by combined mobility and aerodynamic
771 diameter measurements. Part 1: Theory, Aerosol Sci. Technol., 38, 1185-1205,
772 10.1080/027868290903907, 2004.

773   DeCarlo, P. F., Kimmel, J. R., Trimborn, A., Northway, M. J., Jayne, J. T., Aiken, A. C.,
774   Gonin, M., Fuhrer, K., Horvath, T., Docherty, K. S., Worsnop, D. R., and Jimenez, J. L.:
775   Field-deployable, high-resolution, time-of-flight aerosol mass spectrometer, Analytical
776   Chemistry, 78, 8281-8289, 10.1021/ac061249n, 2006.

777   Donahue, N. M., Robinson, A. L., Stanier, C. O., and Pandis, S. N.: Coupled partitioning,
778   dilution, and chemical aging of semivolatile organics, Environmental Science &
779   Technology, 40, 2635-2643, 10.1021/es052297c, 2006.

780   Donahue, N. M., Epstein, S. A., Pandis, S. N., and Robinson, A. L.: A two-dimensional
781   volatility basis set: 1. organic-aerosol mixing thermodynamics, Atmospheric Chemistry
782   and Physics, 11, 3303-3318, 10.5194/acp-11-3303-2011, 2011.

783   Ehn, M., Thornton, J. A., Kleist, E., Sipila, M., Junninen, H., Pullinen, I., Springer, M.,
784   Rubach, F., Tillmann, R., Lee, B., Lopez-Hilfiker, F., Andres, S., Acir, I. H., Rissanen,
785   M., Jokinen, T., Schobesberger, S., Kangasluoma, J., Kontkanen, J., Nieminen, T.,
786   Kurten, T., Nielsen, L. B., Jorgensen, S., Kjaergaard, H. G., Canagaratna, M., Dal Maso,
787   M., Berndt, T., Petaja, T., Wahner, A., Kerminen, V. M., Kulmala, M., Worsnop, D. R.,
788   Wildt, J., and Mentel, T. F.: A large source of low-volatility secondary organic aerosol,
789   Nature, 506, 476-479, 10.1038/nature13032, 2014.

790   Fry, J. L., Kiendler-Scharr, A., Rollins, A. W., Wooldridge, P. J., Brown, S. S., Fuchs,
791   H., Dube, W., Mensah, A., dal Maso, M., Tillmann, R., Dorn, H. P., Brauers, T., and
792   Cohen, R. C.: Organic nitrate and secondary organic aerosol yield from NO3 oxidation of
793   beta-pinene evaluated using a gas-phase kinetics/aerosol partitioning model, Atmospheric
794   Chemistry and Physics, 9, 1431-1449, 2009.

795   Fry, J. L., Draper, D. C., Barsanti, K. C., Smith, J. N., Ortega, J., Winkler, P. M., Lawler,
796   M. J., Brown, S. S., Edwards, P. M., Cohen, R. C., and Lee, L.: Secondary Organic
797   Aerosol Formation and Organic Nitrate Yield from NO3 Oxidation of Biogenic
798   Hydrocarbons, Environmental Science & Technology, 48, 11944-11953,
799   10.1021/es502204x, 2014.

800   Gao, S., Ng, N. L., Keywood, M., Varutbangkul, V., Bahreini, R., Nenes, A., He, J. W.,
801   Yoo, K. Y., Beauchamp, J. L., Hodyss, R. P., Flagan, R. C., and Seinfeld, J. H.: Particle
802   phase acidity and oligomer formation in secondary organic aerosol, Environmental
803   Science & Technology, 38, 6582-6589, 10.1021/es049125k, 2004.

804   Grieshop, A. P., Donahue, N. M., and Robinson, A. L.: Is the gas-particle partitioning in
805   alpha-pinene secondary organic aerosol reversible?, Geophys. Res. Lett., 34, n/a-n/a,
806   10.1029/2007GL029987, 2007.

807   Griffin, R. J., Cocker, D. R., Flagan, R. C., and Seinfeld, J. H.: Organic aerosol formation
808   from the oxidation of biogenic hydrocarbons, J. Geophys. Res.-Atmos., 104, 3555-3567,
809   10.1029/1998jd100049, 1999.

810   Guenther, A. B., Jiang, X., Heald, C. L., Sakulyanontvittaya, T., Duhl, T., Emmons, L.
811   K., and Wang, X.: The Model of Emissions of Gases and Aerosols from Nature version
812   2.1 (MEGAN2.1): an extended and updated framework for modeling biogenic emissions,
813   Geoscientific Model Development, 5, 1471-1492, 10.5194/gmd-5-1471-2012, 2012.

814   Hallquist, M., Wenger, J. C., Baltensperger, U., Rudich, Y., Simpson, D., Claeys, M.,
815   Dommen, J., Donahue, N. M., George, C., Goldstein, A. H., Hamilton, J. F., Herrmann,
816   H., Hoffmann, T., Iinuma, Y., Jang, M., Jenkin, M. E., Jimenez, J. L., Kiendler-Scharr,
817   A., Maenhaut, W., McFiggans, G., Mentel, T. F., Monod, A., Prevot, A. S. H., Seinfeld,
818   J. H., Surratt, J. D., Szmigielski, R., and Wildt, J.: The formation, properties and impact
819   of secondary organic aerosol: current and emerging issues, Atmospheric Chemistry and
820   Physics, 9, 5155-5236, 2009.

821   Henry, K. M., Lohaus, T., and Donahue, N. M.: Organic Aerosol Yields from alpha-
822   Pinene Oxidation: Bridging the Gap between First-Generation Yields and Aging
823   Chemistry, Environmental Science & Technology, 46, 12347-12354, 10.1021/es302060y,
824   2012.

825   Hildebrandt, L., Donahue, N. M., and Pandis, S. N.: High formation of secondary organic
826   aerosol from the photo-oxidation of toluene, Atmospheric Chemistry and Physics, 9,
827   2973-2986, 2009.

828   Hoffmann, T., Odum, J. R., Bowman, F., Collins, D., Klockow, D., Flagan, R. C., and
829   Seinfeld, J. H.: Formation of organic aerosols from the oxidation of biogenic
830   hydrocarbons, Journal of Atmospheric Chemistry, 26, 189-222,
831   10.1023/a:1005734301837, 1997.

832   Kanakidou, M., Seinfeld, J. H., Pandis, S. N., Barnes, I., Dentener, F. J., Facchini, M. C.,
833   Van Dingenen, R., Ervens, B., Nenes, A., Nielsen, C. J., Swietlicki, E., Putaud, J. P.,
834   Balkanski, Y., Fuzzi, S., Horth, J., Moortgat, G. K., Winterhalter, R., Myhre, C. E. L.,
835   Tsigaridis, K., Vignati, E., Stephanou, E. G., and Wilson, J.: Organic aerosol and global
836   climate modelling: a review, Atmospheric Chemistry and Physics, 5, 1053-1123, 2005.

837   Keywood, M. D., Varutbangkul, V., Bahreini, R., Flagan, R. C., and Seinfeld, J. H.:
838   Secondary organic aerosol formation from the ozonolysis of cycloalkenes and related
839   compounds, Environmental Science & Technology, 38, 4157-4164, 10.1021/es035363o,
840   2004.

841   Kokkola, H., Yli-Pirila, P., Vesterinen, M., Korhonen, H., Keskinen, H., Romakkaniemi,
842   S., Hao, L., Kortelainen, A., Joutsensaari, J., Worsnop, D. R., Virtanen, A., and Lehtinen,
843   K. E. J.: The role of low volatile organics on secondary organic aerosol formation,
844   Atmospheric Chemistry and Physics, 14, 1689-1700, 10.5194/acp-14-1689-2014, 2014.

845   Kostenidou, E., Pathak, R. K., and Pandis, S. N.: An algorithm for the calculation of
846   secondary organic aerosol density combining AMS and SMPS data, Aerosol Sci.
847   Technol., 41, 1002-1010, 10.1080/02786820701666270, 2007.

848   Kristensen, K., Cui, T., Zhang, H., Gold, A., Glasius, M., and Surratt, J. D.: Dimers in
849   alpha-pinene secondary organic aerosol: effect of hydroxyl radical, ozone, relative
850   humidity and aerosol acidity, Atmospheric Chemistry and Physics, 14, 4201-4218,
851   10.5194/acp-14-4201-2014, 2014.

852   Kroll, J. H., Chan, A. W. H., Ng, N. L., Flagan, R. C., and Seinfeld, J. H.: Reactions of
853   semivolatile organics and their effects on secondary organic aerosol formation,
854   Environmental Science & Technology, 41, 3545-3550, 10.1021/es062059x, 2007.

855   Kuwata, M., and Martin, S. T.: Phase of atmospheric secondary organic material affects
856   its reactivity, Proc. Natl. Acad. Sci. U. S. A., 109, 17354-17359,
857   10.1073/pnas.1209071109, 2012.

858   La, Y. S., Camredon, M., Ziemann, P. J., Valorso, R., Matsunaga, A., Lannuque, V., Lee-
859   Taylor, J., Hodzic, A., Madronich, S., and Aumont, B.: Impact of chamber wall loss of
860   gaseous organic compounds on secondary organic aerosol formation: explicit modeling
861   of SOA formation from alkane and alkene oxidation, Atmos. Chem. Phys., 16, 1417-
862   1431, 10.5194/acp-16-1417-2016, 2016.

863   Loza, C. L., Chan, A. W. H., Galloway, M. M., Keutsch, F. N., Flagan, R. C., and
864   Seinfeld, J. H.: Characterization of Vapor Wall Loss in Laboratory Chambers,
865   Environmental Science & Technology, 44, 5074-5078, 10.1021/es100727v, 2010.

866   Loza, C. L., Chhabra, P. S., Yee, L. D., Craven, J. S., Flagan, R. C., and Seinfeld, J. H.:
867   Chemical aging of m-xylene secondary organic aerosol: laboratory chamber study,
868   Atmospheric Chemistry and Physics, 12, 151-167, 10.5194/acp-12-151-2012, 2012.

869   Matsunaga, A., and Ziemann, P. J.: Gas-Wall Partitioning of Organic Compounds in a
870   Teflon Film Chamber and Potential Effects on Reaction Product and Aerosol Yield
871   Measurements, Aerosol Sci. Technol., 44, 881-892, 10.1080/02786826.2010.501044,
872   2010.

873   McMurry, P. H., and Grosjean, D.: Gas and Aerosol Wall Losses in Teflon Film Smog
874   Chambers, Environmental Science & Technology, 19, 1176-1182, 10.1021/es00142a006,
875   1985.

876   McMurry, P. H., and Rader, D. J.: Aerosol Wall Losses in Electrically Charged
877   Chambers, Aerosol Sci. Technol., 4, 249-268, 10.1080/02786828508959054, 1985.

878   McVay, R. C., Cappa, C. D., and Seinfeld, J. H.: Vapor-Wall Deposition in Chambers:
879   Theoretical Considerations, Environmental Science & Technology, 48, 10251-10258,
880   10.1021/es502170j, 2014.

881 McVay, R. C., Zhang, X., Aumont, B., Valorso, R., Camredon, M., La, Y. S., Wennberg,
882 P. O., and Seinfeld, J. H.: SOA formation from the photooxidation of α-pinene:
883 systematic exploration of the simulation of chamber data, Atmos. Chem. Phys., 16, 2785-
884 2802, 10.5194/acp-16-2785-2016, 2016.

885 Miles, R. E. H., Reid, J. P., and Riipinen, I.: Comparison of Approaches for Measuring
886 the Mass Accommodation Coefficient for the Condensation of Water and Sensitivities to
887 Uncertainties in Thermophysical Properties, J. Phys. Chem. A, 116, 10810-10825,
888 10.1021/jp3083858, 2012.

889 Ng, N. L., Kroll, J. H., Keywood, M. D., Bahreini, R., Varutbangkul, V., Flagan, R. C.,
890 Seinfeld, J. H., Lee, A., and Goldstein, A. H.: Contribution of first- versus second-
891 generation products to secondary organic aerosols formed in the oxidation of biogenic
892 hydrocarbons, Environmental Science & Technology, 40, 2283-2297,
893 10.1021/es052269u, 2006.

894 Ng, N. L., Kroll, J. H., Chan, A. W. H., Chhabra, P. S., Flagan, R. C., and Seinfeld, J. H.:
895 Secondary organic aerosol formation from m-xylene, toluene, and benzene, Atmospheric
896 Chemistry and Physics, 7, 3909-3922, 2007.

897 Odum, J. R., Hoffmann, T., Bowman, F., Collins, D., Flagan, R. C., and Seinfeld, J. H.:
898 Gas/Particle Partitioning and Secondary Organic Aerosol Yields, Environmental Science
899 & Technology, 30, 2580-2585, 10.1021/es950943+, 1996.

900 Odum, J. R., Jungkamp, T. P. W., Griffin, R. J., Flagan, R. C., and Seinfeld, J. H.: The
901 atmospheric aerosol-forming potential of whole gasoline vapor, Science, 276, 96-99,
902 10.1126/science.276.5309.96, 1997a.

903 Odum, J. R., Jungkamp, T. P. W., Griffin, R. J., Forstner, H. J. L., Flagan, R. C., and
904 Seinfeld, J. H.: Aromatics, reformulated gasoline, and atmospheric organic aerosol
905 formation, Environmental Science & Technology, 31, 1890-1897, 10.1021/es960535l,
906 1997b.

907 Pathak, R. K., Presto, A. A., Lane, T. E., Stanier, C. O., Donahue, N. M., and Pandis, S.
908 N.: Ozonolysis of alpha-pinene: parameterization of secondary organic aerosol mass
909 fraction, Atmospheric Chemistry and Physics, 7, 3811-3821, 2007a.

910 Pathak, R. K., Stanier, C. O., Donahue, N. M., and Pandis, S. N.: Ozonolysis of alpha-
911 pinene at atmospherically relevant concentrations: Temperature dependence of aerosol
912 mass fractions (yields), J. Geophys. Res.-Atmos., 112, 8, 10.1029/2006jd007436, 2007b.

913 Perraud, V., Bruns, E. A., Ezell, M. J., Johnson, S. N., Yu, Y., Alexander, M. L.,
914 Zelenyuk, A., Imre, D., Chang, W. L., Dabdub, D., Pankow, J. F., and Finlayson-Pitts, B.
915 J.: Nonequilibrium atmospheric secondary organic aerosol formation and growth, Proc.
916 Natl. Acad. Sci. U. S. A., 109, 2836-2841, 10.1073/pnas.1119909109, 2012.

917 Pierce, J. R., Engelhart, G. J., Hildebrandt, L., Weitkamp, E. A., Pathak, R. K., Donahue,
918 N. M., Robinson, A. L., Adams, P. J., and Pandis, S. N.: Constraining particle evolution
919 from wall losses, coagulation, and condensation-evaporation in smog-chamber
920 experiments: Optimal estimation based on size distribution measurements, Aerosol Sci.
921 Technol., 42, 1001-1015, 10.1080/02786820802389251, 2008.

922 Presto, A. A., Hartz, K. E. H., and Donahue, N. M.: Secondary organic aerosol
923 production from terpene ozonolysis. 2. Effect of NOx concentration, Environmental
924 Science & Technology, 39, 7046-7054, 10.1021/es050400s, 2005.

925 Presto, A. A., and Donahue, N. M.: Investigation of alpha-pinene plus ozone secondary
926 organic aerosol formation at low total aerosol mass, Environmental Science &
927 Technology, 40, 3536-3543, 10.1021/es052203z, 2006.

928 Pye, H. O. T., Chan, A. W. H., Barkley, M. P., and Seinfeld, J. H.: Global modeling of
929 organic aerosol: the importance of reactive nitrogen (NOx and NO3), Atmospheric
930 Chemistry and Physics, 10, 11261-11276, 10.5194/acp-10-11261-2010, 2010.

931 Renbaum-Wolff, L., Grayson, J. W., Bateman, A. P., Kuwata, M., Sellier, M., Murray, B.
932 J., Shilling, J. E., Martin, S. T., and Bertram, A. K.: Viscosity of alpha-pinene secondary

933   organic material and implications for particle growth and reactivity, Proc. Natl. Acad.
934   Sci. U. S. A., 110, 8014-8019, 10.1073/pnas.1219548110, 2013.

935   Saleh, R., Donahue, N. M., and Robinson, A. L.: Time Scales for Gas-Particle
936   Partitioning Equilibration of Secondary Organic Aerosol Formed from Alpha-Pinene
937   Ozonolysis, Environmental Science & Technology, 47, 5588-5594, 10.1021/es400078d,
938   2013.

939   Saukko, E., Lambe, A. T., Massoli, P., Koop, T., Wright, J. P., Croasdale, D. R.,
940   Pedernera, D. A., Onasch, T. B., Laaksonen, A., Davidovits, P., Worsnop, D. R., and
941   Virtanen, A.: Humidity-dependent phase state of SOA particles from biogenic and
942   anthropogenic precursors, Atmospheric Chemistry and Physics, 12, 7517-7529,
943   10.5194/acp-12-7517-2012, 2012.

944   Saunders, S. M., Jenkin, M. E., Derwent, R. G., and Pilling, M. J.: Protocol for the
945   development of the Master Chemical Mechanism, MCM v3 (Part A): tropospheric
946   degradation of non-aromatic volatile organic compounds, Atmos. Chem. Phys., 3, 161-
947   180, 10.5194/acp-3-161-2003, 2003.

948   Seinfeld, J. H., and Pandis, S. N.: Atmospheric chemistry and physics : from air pollution
949   to climate change, 2nd ed., Wiley, Hoboken, N.J., xxviii, 1203 p. pp., 2006.

950   Shilling, J. E., Chen, Q., King, S. M., Rosenoern, T., Kroll, J. H., Worsnop, D. R.,
951   McKinney, K. A., and Martin, S. T.: Particle mass yield in secondary organic aerosol
952   formed by the dark ozonolysis of alpha-pinene, Atmospheric Chemistry and Physics, 8,
953   2073-2088, 2008.

954   Shilling, J. E., Chen, Q., King, S. M., Rosenoern, T., Kroll, J. H., Worsnop, D. R.,
955   DeCarlo, P. F., Aiken, A. C., Sueper, D., Jimenez, J. L., and Martin, S. T.: Loading-
956   dependent elemental composition of alpha-pinene SOA particles, Atmospheric Chemistry
957   and Physics, 9, 771-782, 2009.

958   Shiraiwa, M., and Seinfeld, J. H.: Equilibration timescale of atmospheric secondary
959   organic aerosol partitioning, Geophys. Res. Lett., 39, 6, 10.1029/2012gl054008, 2012.

960   Song, C., Zaveri, R. A., Alexander, M. L., Thornton, J. A., Madronich, S., Ortega, J. V.,
961   Zelenyuk, A., Yu, X. Y., Laskin, A., and Maughan, D. A.: Effect of hydrophobic primary
962   organic aerosols on secondary organic aerosol formation from ozonolysis of alpha-
963   pinene, Geophys. Res. Lett., 34, 5, 10.1029/2007gl030720, 2007.

964   Stanier, C. O., Pathak, R. K., and Pandis, S. N.: Measurements of the volatility of
965   aerosols from alpha-piniene ozonolysis, Environmental Science & Technology, 41, 2756-
966   2763, 10.1021/es0519280, 2007.

967   Tsigaridis, K., Daskalakis, N., Kanakidou, M., Adams, P. J., Artaxo, P., Bahadur, R.,
968   Balkanski, Y., Bauer, S. E., Bellouin, N., Benedetti, A., Bergman, T., Berntsen, T. K.,
969   Beukes, J. P., Bian, H., Carslaw, K. S., Chin, M., Curci, G., Diehl, T., Easter, R. C.,
970   Ghan, S. J., Gong, S. L., Hodzic, A., Hoyle, C. R., Iversen, T., Jathar, S., Jimenez, J. L.,
971   Kaiser, J. W., Kirkevåg, A., Koch, D., Kokkola, H., Lee, Y. H., Lin, G., Liu, X., Luo, G.,
972   Ma, X., Mann, G. W., Mihalopoulos, N., Morcrette, J. J., Müller, J. F., Myhre, G.,
973   Myriokefalitakis, S., Ng, N. L., O'Donnell, D., Penner, J. E., Pozzoli, L., Pringle, K. J.,
974   Russell, L. M., Schulz, M., Sciare, J., Seland, Ø., Shindell, D. T., Sillman, S., Skeie, R.
975   B., Spracklen, D., Stavrakou, T., Steenrod, S. D., Takemura, T., Tiitta, P., Tilmes, S.,
976   Tost, H., van Noije, T., van Zyl, P. G., von Salzen, K., Yu, F., Wang, Z., Wang, Z.,
977   Zaveri, R. A., Zhang, H., Zhang, K., Zhang, Q., and Zhang, X.: The AeroCom evaluation
978   and intercomparison of organic aerosol in global models, Atmos. Chem. Phys., 14,
979   10845-10895, 10.5194/acp-14-10845-2014, 2014.

980   Vaden, T. D., Song, C., Zaveri, R. A., Imre, D., and Zelenyuk, A.: Morphology of mixed
981   primary and secondary organic particles and the adsorption of spectator organic gases
982   during aerosol formation, Proc. Natl. Acad. Sci. U. S. A., 107, 6658-6663,
983   10.1073/pnas.0911206107, 2010.

984   Vaden, T. D., Imre, D., Beranek, J., Shrivastava, M., and Zelenyuk, A.: Evaporation
985   kinetics and phase of laboratory and ambient secondary organic aerosol, Proc. Natl.
986   Acad. Sci. U. S. A., 108, 2190-2195, 10.1073/pnas.1013391108, 2011.

987   Virtanen, A., Joutsensaari, J., Koop, T., Kannosto, J., Yli-Pirila, P., Leskinen, J., Makela,
988   J. M., Holopainen, J. K., Poschl, U., Kulmala, M., Worsnop, D. R., and Laaksonen, A.:
989   An amorphous solid state of biogenic secondary organic aerosol particles, Nature, 467,
990   824-827, 10.1038/nature09455, 2010.

991   Virtanen, A., Kannosto, J., Kuuluvainen, H., Arffman, A., Joutsensaari, J., Saukko, E.,
992   Hao, L., Yli-Pirila, P., Tiitta, P., Holopainen, J. K., Keskinen, J., Worsnop, D. R., Smith,
993   J. N., and Laaksonen, A.: Bounce behavior of freshly nucleated biogenic secondary
994   organic aerosol particles, Atmospheric Chemistry and Physics, 11, 8759-8766,
995   10.5194/acp-11-8759-2011, 2011.

996   Weitkamp, E. A., Sage, A. M., Pierce, J. R., Donahue, N. M., and Robinson, A. L.:
997   Organic aerosol formation from photochemical oxidation of diesel exhaust in a smog
998   chamber, Environmental Science & Technology, 41, 6969-6975, 10.1021/es070193r,
999   2007.

1000 Yeh, G. K., and Ziemann, P. J.: Alkyl Nitrate Formation from the Reactions of C-8-C-14
1001 n-Alkanes with OH Radicals in the Presence of NOx: Measured Yields with Essential
1002 Corrections for Gas-Wall Partitioning, J. Phys. Chem. A, 118, 8147-8157,
1003 10.1021/jp500631v, 2014.

1004 Yeh, G. K., and Ziemann, P. J.: Gas-Wall Partitioning of Oxygenated Organic
1005 Compounds: Measurements, Structure-Activity Relationships, and Correlation with Gas
1006 Chromatographic Retention Factor, Aerosol Sci. Technol., 49, 726-737,
1007 10.1080/02786826.2015.1068427, 2015.

1008 Zhang, X., Pandis, S. N., and Seinfeld, J. H.: Diffusion-Limited Versus Quasi-
1009 Equilibrium Aerosol Growth, Aerosol Sci. Technol., 46, 874-885,
1010 10.1080/02786826.2012.679344, 2012.

1011 Zhang, X., Cappa, C. D., Jathar, S. H., McVay, R. C., Ensberg, J. J., Kleeman, M. J., and
1012 Seinfeld, J. H.: Influence of vapor wall loss in laboratory chambers on yields of
1013 secondary organic aerosol, Proc. Natl. Acad. Sci. U. S. A., 111, 5802-5807,
1014 10.1073/pnas.1404727111, 2014.

1015   Zhang, X., Schwantes, R. H., McVay, R. C., Lignell, H., Coggon, M. M., Flagan, R. C.,

1016   and Seinfeld, J. H.: Vapor wall deposition in Teflon chambers, Atmospheric Chemistry

1017   and Physics, 15, 4197-4214, 10.5194/acp-15-4197-2015, 2015a.

1018   Zhang, X., McVay, R. C., Huang, D. D., Dalleska, N. F., Aumont, B., Flagan, R. C., and

1019   Seinfeld, J. H.: Formation and evolution of molecular products in alpha-pinene secondary

1020   organic   aerosol,   Proc.   Natl.   Acad.   Sci.   U.   S.   A.,   112,   14168-14173,

1021   10.1073/pnas.1517742112, 2015b.

1022

1023

1024

1025

1026

1027

1028

1029

1030

1031

1032

1033

1034

1035

1036

1037

1038   **Table 1:** Experimental conditions and results for the α-pinene ozonolysis experiments

Experiment	Initial Seed Surface Area (μm^2 cm^{-3})	Initial [α-pinene][a] (μg m^{-3})	ΔM_0[b] (μg m^{-3})	SOA Mass Yield[c] (%)
100 ppb O_3 nucleation	0	290.2±23.2	62.0±1.2[d]	22.6±1.9
100 ppb O_3 low AS	1130	280.5±22.4	63.0±0.8[d]	23.3±1.9
100 ppb O_3 high AS	2700	238.7±19.1	50.6±1.6[d]	23.3±1.9
500 ppb O_3 nucleation	0	274.4±21.9	87.3±0.3[e]	31.8±2.5
500 ppb O_3 low AS	1300	264.9±21.2	75.7±0.6[e]	28.6±2.3
500 ppb O_3 high AS	2720	236.1±18.9	66.3±1.9[e]	28.1±2.4

1039   [a]Concentration of α-pinene injected into the chamber. All the α-pinene reacted in the 500
1040   ppb O_3 experiments, but not the 100 ppb O_3 experiments.
1041   [b]Uncertainties in the peak SOA mass concentration (ΔM_0) are calculated from one
1042   standard deviation of the aerosol volume as measured by the scanning mobility particle
1043   sizer.
1044   [c]SOA mass yields at peak SOA growth are reported.
1045   [d]The SOA mass concentration is calculated using the density = 1.39 g cm^{-3} obtained from
1046   the 100 ppb O_3 nucleation experiment.
1047   [e]The SOA mass concentration is calculated using the density = 1.37 g cm^{-3} obtained from
1048   the 500 ppb O_3 nucleation experiment.
1049

1050

1051

1052

1053

1054

1055

1056

1057

1058

1059

1060

1061   **Table 2:** Coupled vapor-particle dynamics model parameters

Parameter	Definition	Value
α_p	Vapor-particle mass accommodation coefficient	1
α_w	Vapor-wall mass accommodation coefficient	10^{-6}
τ_{olig}	Timescale of oligomerization	4 h
C^*	Saturation vapor pressures and branching ratios of oxidation products	[0.57 ($>10^3$), 0.35 (10^2), 0.04 (10), 0.015 (1) and 0.025 (0.1)]
D_i	Gas-phase molecular diffusivity	3×10^{-6} m^2 s^{-1}
A/V	Surface area-to-volume ratio of the chamber	2.5 m^{-1}
C_w	Equivalent organic mass concentration in the wall	10 mg m^{-3}
k_e	Eddy diffusion coefficient	0.03 s^{-1}
M_i	Molecular weight of the diffusing gas-phase molecule i	168, 184, 192, 200 and 216 g mole^{-1}
M_{init}	Initially absorbing organic material in seed aerosol	0.01 μg m^{-3}
P	Pressure	1×10^5 Pa
T	Temperature	298 K
ρ_{seed}	Density of inorganic seed	1700 kg m^{-3}
ρ_{org}	Density of organic material on seed particle	1300 kg m^{-3}

1062

1063

1064

1065

1066

1067

1068
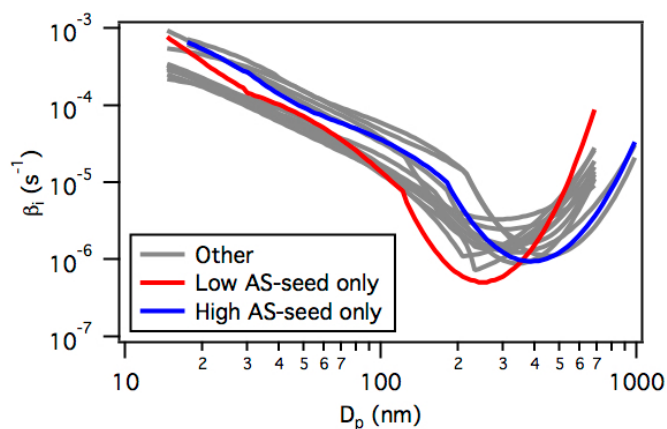
1069

1070   **Figure 1:** Particle wall deposition coefficients (β_i) measured during the low AS-seed
1071   only and high AS-seed only experiments in GTEC. Also shown are the particle wall
1072   deposition coefficients (labeled "Other") measured in previous routine monthly AS-seed
1073   only experiments in the chamber. These previous routine monthly AS-seed only
1074   experiments were performed using either a 0.008 M AS or a 0.1 M AS solution.

1075
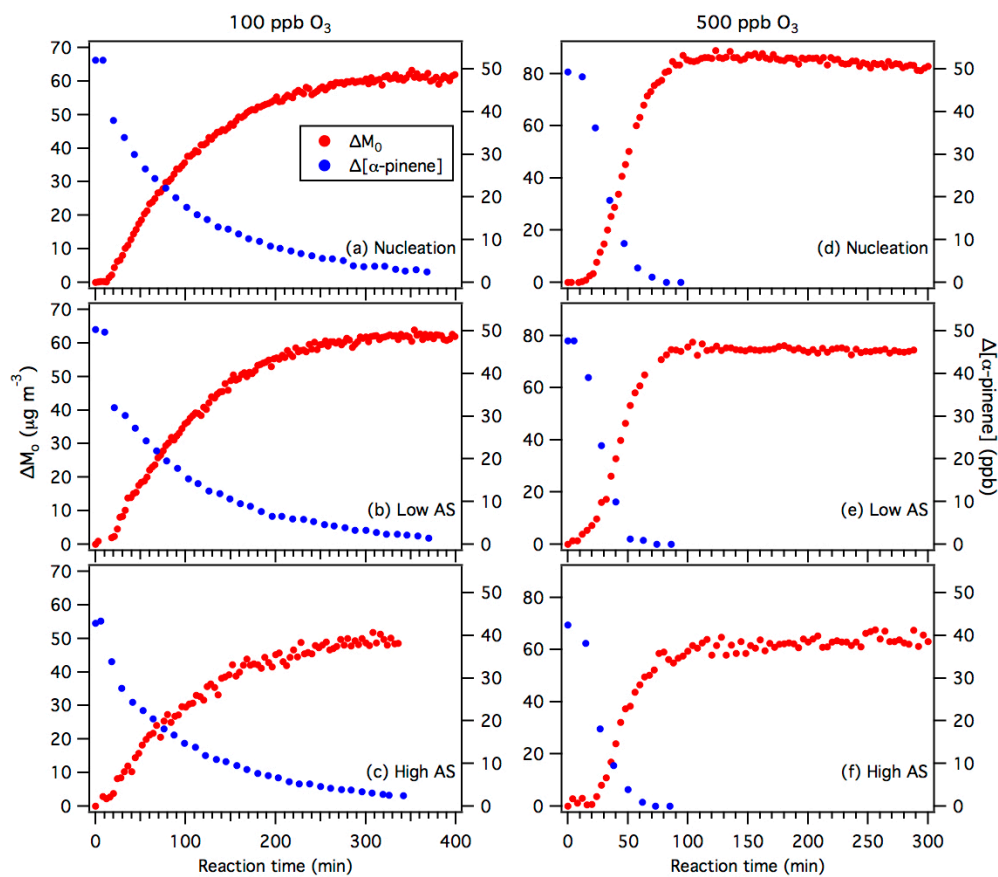
Figure 2: Reaction profiles of the α-pinene ozonolysis experiments. Panels (a), (b) and (c) show results from the nucleation, low AS and high AS 100 ppb O_3 experiments, respectively. Panels (d), (e) and (f) show results from the nucleation, low AS and high AS 500 ppb O_3 experiments, respectively. As explained in the main text, the SOA mass concentrations (ΔM_o) for the nucleation and low AS experiments are obtained using the particle wall rates obtained from the low AS-seed only experiments, while the SOA mass concentrations (ΔM_o) for the high AS-seed experiments are obtained using the particle wall rates obtained from the high AS-seed only experiments.
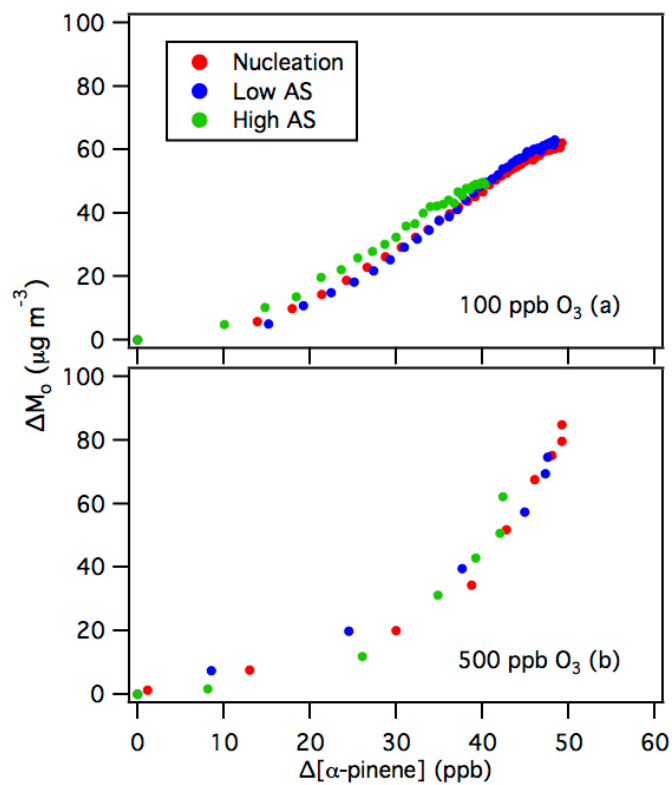
1086

1087 **Figure 3:** Time-dependent SOA growth curves for α-pinene ozonolysis. Panels (a) and
1088 (b) show 10 min-averaged results from the 100 ppb and 500 ppb O₃ experiments,
1089 respectively. Only SOA growth data up to the point of SOA peak growth are shown.

1090
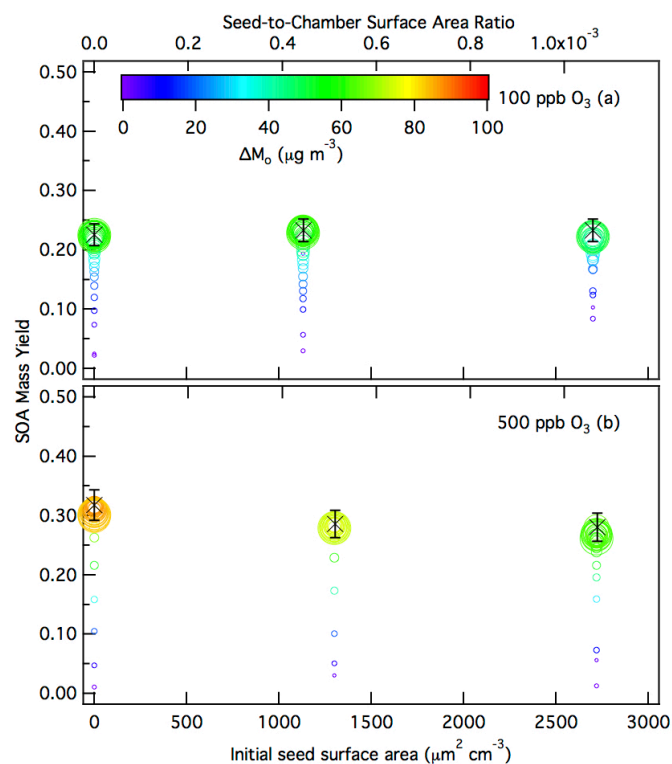
Figure 4: 10 min-averaged SOA mass yields over the course of an α-pinene ozonolysis experiment as a function of initial total AS seed surface area concentration for the (a) 100 ppb O_3 experiments, and (b) 500 ppb O_3 experiments. Symbol color indicates the SOA mass concentration and symbol size indicates the time after O_3 is injected into the chamber. The ✕ symbols are the SOA mass yields at peak SOA growth obtained from the experimental data. The y-axis error bars represent the uncertainty in the SOA mass yield at peak SOA growth, which originates from the α-pinene injection and the aerosol volume concentration measured by the SMPS at peak SOA growth (one standard deviation).

1102
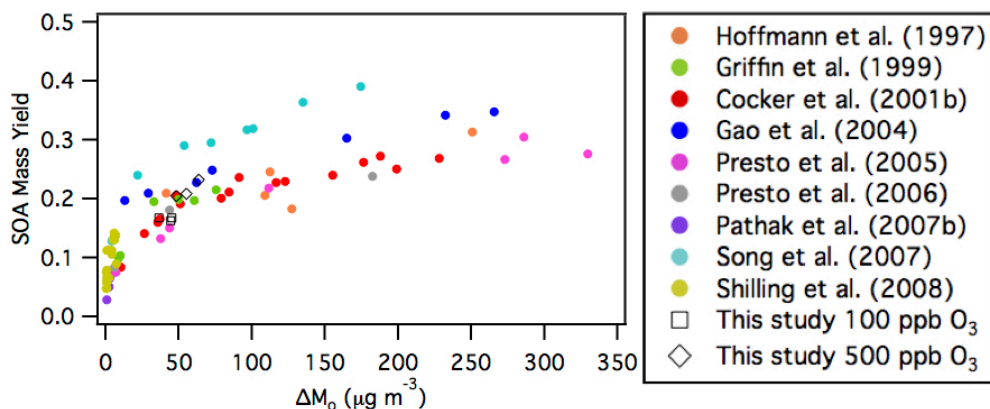
1103

Figure 5: Comparison of SOA mass yields obtained in this study to those of previous
dark α-pinene ozonolysis studies (Table S2). The SOA mass yields and concentrations of
majority of these previous studies (Hoffmann et al., 1997; Griffin et al., 1999; Cocker et
al., 2001b; Gao et al., 2004; Presto et al., 2005; Presto et al. 2006; Pathak et al., 2007b;
Song et al., 2007) were previously compiled by Shilling et al (2008). Similar to Shilling
et al. (2008), all the data shown here (including those reported in this study) have been
adjusted using an organic density of 1.0 g cm^{-3}, and to 298 K using a temperature
correction of 1.6 % per K, as recommended by Pathak et al. (2007b) to facilitate easier
comparison among the different studies.
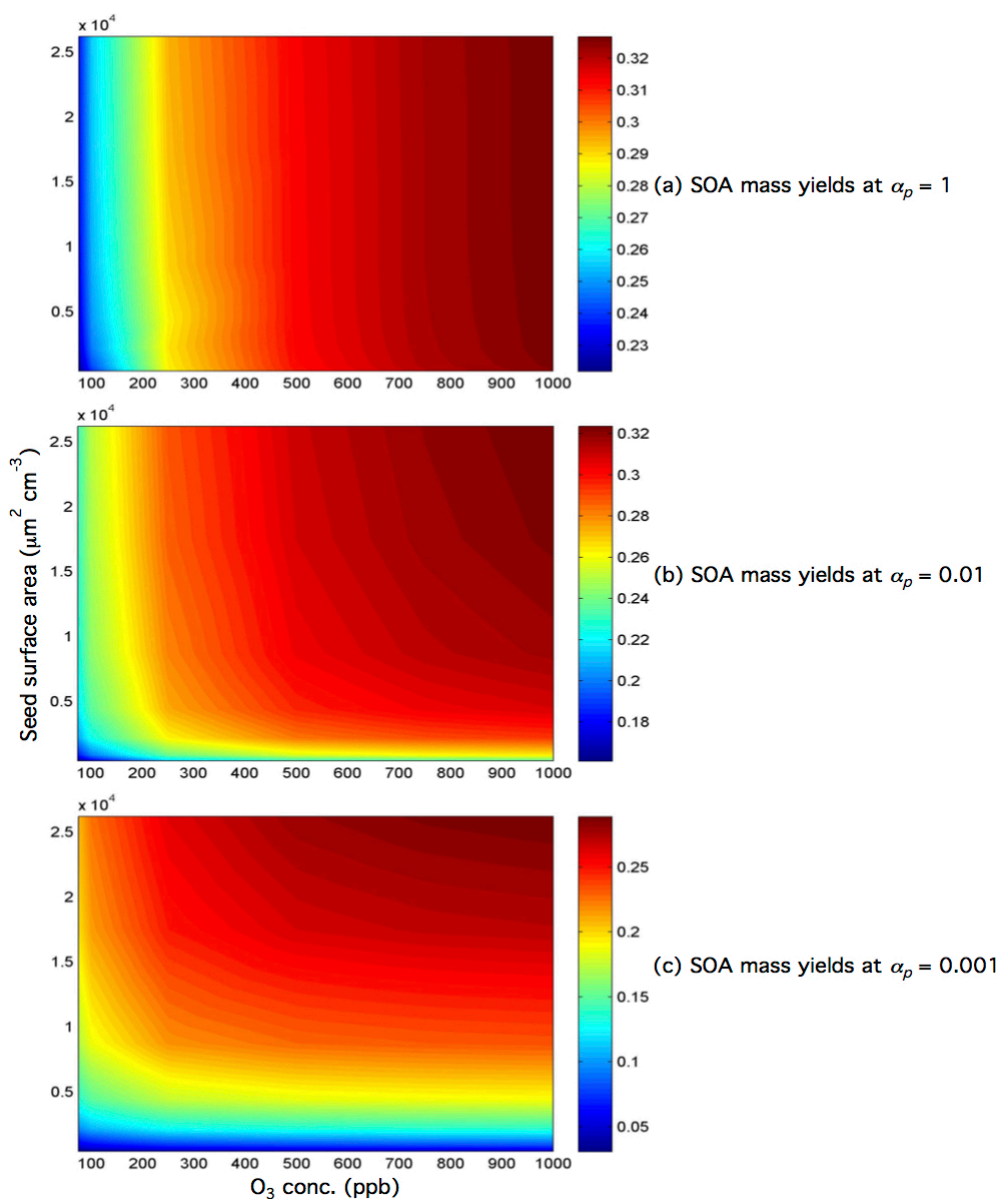
Figure 6: SOA mass yields at peak SOA growth as a function of both the seed surface area and O_3 concentration for $\alpha_p = 1$, 0.01, and 0.001. The SOA mass yields at peak SOA growth are indicated by colors and contours. Note that the color bars for panels (a), (b) and (c) have different SOA mass yield ranges. Simulations were carried out using the branching ratios, oligomerization rate, and vapor wall deposition rate parameters obtained in this study. The initial α-pinene concentration was set to 50 ppb, and a fixed O_3 concentration was used in place of a linear injection.